Gastroenterology 2023;164:392–406

GI CANCER

N-glycosylation Regulates Intrinsic IFN-γ Resistance in Colorectal Cancer: Implications for Immunotherapy

Julia Krug,[1] Gabriele Rodrian,[1] Katja Petter,[1] Hai Yang,[2] Svetlana Khoziainova,[3,4] Wei Guo,[3] Alan Bénard,[5] Susanne Merkel,[5] Susan Gellert,[6] Simone Maschauer,[7] Monika Spermann,[1] Maximilian Waldner,[8] Peter Bailey,[9] Christian Pilarsky,[2] Andrea Liebl,[1] Philipp Tripal,[1] Jan Christoph,[10] Elisabeth Naschberger,[1] Roland Croner,[11] Vera S. Schellerer,[5] Christoph Becker,[8] Arndt Hartmann,[12] Thomas Tüting,[6] Olaf Prante,[7] Robert Grützmann,[5] Sergei I. Grivennikov,[3,4] Michael Stürzl,[1,13,§] and Nathalie Britzen-Laurent[1,2,§]

[1]Division of Molecular and Experimental Surgery, Department of Surgery, Universitätsklinikum Erlangen, Friedrich-Alexander-Universität Erlangen-Nürnberg (FAU), Erlangen, Germany; [2]Division of Surgical Research, Department of Surgery, Universitätsklinikum Erlangen, Friedrich-Alexander-Universität Erlangen-Nürnberg (FAU), Erlangen, Germany; [3]Cancer Prevention and Control Program, Fox Chase Cancer Center, Philadelphia, Pennsylvania; [4]Department of Medicine, Cedars-Sinai Medical Center, Los Angeles, California; [5]Department of Surgery, Universitätsklinikum Erlangen, Friedrich-Alexander-Universität Erlangen-Nürnberg (FAU), Erlangen, Germany; [6]Laboratory of Experimental Dermatology, Department of Dermatology, University Hospital and Health Campus Immunology Infectiology and Inflammation (GC-I3), Otto-von-Guericke-University, Magdeburg, Germany; [7]Department of Nuclear Medicine, Molecular Imaging and Radiochemistry, Universitätsklinikum Erlangen, Friedrich-Alexander-Universität Erlangen-Nürnberg (FAU), Erlangen, Germany; [8]Department of Medicine I, Universitätsklinikum Erlangen, Friedrich-Alexander-Universität Erlangen-Nürnberg (FAU), Erlangen, Germany; [9]Wolfson Wohl Cancer Research Centre, Institute of Cancer Sciences, University of Glasgow, Glasgow, United Kingdom; [10]Department of Medical Informatics, Friedrich-Alexander-Universität Erlangen-Nürnberg (FAU), Tennenlohe, Germany; [11]Department of General, Visceral, Vascular and Transplant Surgery, University Hospital Magdeburg, Otto-von-Guericke-University, Magdeburg, Germany; [12]Department of Pathology, Universitätsklinikum Erlangen, Friedrich-Alexander-Universität Erlangen-Nürnberg (FAU), Erlangen, Germany; and [13]Comprehensive Cancer Center Erlangen-EMN, Universitätsklinikum Erlangen, Erlangen, Germany

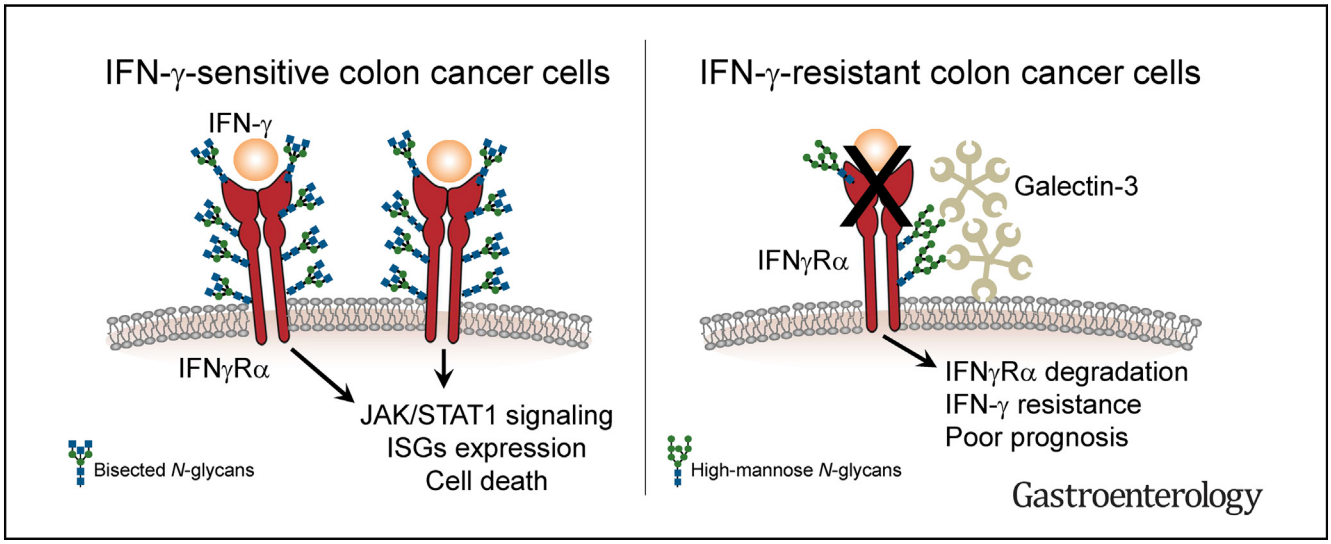

BACKGROUND & AIMS: Advanced colorectal carcinoma (CRC) is characterized by a high frequency of primary immune evasion and refractoriness to immunotherapy. Given the importance of interferon (IFN)-γ in CRC immunosurveillance, we investigated whether and how acquired IFN-γ resistance in tumor cells would promote tumor growth, and whether IFN-γ sensitivity could be restored. **METHODS:** Spontaneous and colitis-associated CRC development was induced in mice with a specific IFN-γ pathway inhibition in intestinal epithelial cells. The influence of IFN-γ pathway gene status and expression on survival was assessed in patients with CRC. The mechanisms underlying IFN-γ resistance were investigated in CRC cell lines. **RESULTS:** The conditional knockout of the IFN-γ receptor in intestinal epithelial cells enhanced spontaneous and colitis-associated colon tumorigenesis in mice, and the loss of IFN-γ receptor α (IFNγRα) expression by tumor cells predicted poor prognosis in patients with CRC. IFNγRα expression was repressed in human CRC cells through changes in *N*-glycosylation, which decreased protein stability via proteasome-dependent degradation, inhibiting IFNγR-

signaling. Downregulation of the bisecting *N*-acetylglucosaminyltransferase III (MGAT3) expression was associated with IFN-γ resistance in all IFN-γ–resistant cells, and highly correlated with low IFNγRα expression in CRC tissues. Both ectopic and pharmacological reconstitution of MGAT3 expression with all-trans retinoic acid increased bisecting *N*-glycosylation, as well as IFNγRα protein stability and signaling. **CONCLUSIONS:** Together, our results demonstrated that tumor-associated changes in *N*-glycosylation destabilize IFNγRα, causing IFN-γ resistance in CRC. IFN-γ sensitivity could be reestablished through the increase in MGAT3 expression, notably via all-trans retinoic acid treatment, providing new prospects for the treatment of immune-resistant CRC.

Keywords: Colon Cancer; Immune Evasion; IFNGR1.

The primary host immune response is an important determinant of the evolution of solid tumors. In colorectal cancer (CRC), the infiltration of T helper 1 and cytotoxic T cells correlates with an increased patient survival and the presence of an interferon (IFN)-γ–driven expression signature.[1,2] The crucial role of IFN-γ in tumor immunosurveillance has been amply documented in preclinical models.[3] IFN-γ is secreted by immune cells, mostly cytotoxic T cells, and can exert long-distance effects in the tumor microenvironment, inducing a sustained IFN-γ response in tumor cells.[4,5] Tumor cell–specific effects of IFN-γ include the inhibition of cell proliferation, the induction of cell death, and an increased immunogenicity.[3,6] IFN-γ binds the ubiquitously expressed IFN-γ receptor (IFNγR) α/β complex and signals through the Janus kinase/signal transducers and activators of transcription (JAK/STAT) signaling pathway. Activation of STAT1 and interferon regulatory factor 1 induces the transcription of interferon-stimulated genes (ISGs).[7] In CRC, the expression of various ISGs has been associated with less aggressive disease.[8–10]

Tumor cells can develop strategies to escape detection and destruction by immune cells. Metastatic CRC is characterized by an increased immune resistance.[11] Enhanced expression of immune checkpoint molecules, such as programmed death ligand 1, is infrequent in CRC. Accordingly, immunotherapy with anti-programmed death 1 (anti-PD-1) antibodies only led to an objective response in a small subgroup of microsatellite instable CRCs.[12,13] This indicates that, in the large majority of CRCs, primary immune escape involves mechanisms other than immune checkpoint activation. We previously observed the selective loss of ISG expression in CRC tumor cells compared with the stroma,[14] suggesting that resistance to IFN-γ might be involved in primary immune evasion of CRC. This is supported by the fact that some colorectal cell lines are insensitive to IFN-γ treatment.[14,15] In addition, the treatment of patients with CRC with IFN-γ has yielded a low response rate.[16–18]

Inactivating frameshift mutations of JAK1 have been reported in CRC with microsatellite instability

WHAT YOU NEED TO KNOW

BACKGROUND AND CONTEXT

During tumor progression, colorectal carcinomas develop intrinsic immune evasion. We investigated to which extent a tumor cell acquired interferon-γ resistance participates in tumor development.

NEW FINDINGS

Interferon-γ receptor expression knockout in intestinal tumor cells fosters colon tumorigenesis in mice. *MGAT3*/GnT-III–mediated bisecting *N*-glycosylation regulates interferon-γ receptor α protein stability and function, modulating interferon-γ sensitivity in colorectal cancer cells.

LIMITATIONS

A direct in-situ measure of interferon-γ receptor α *N*-glycosylation could not be performed because of technical limitations.

CLINICAL RESEARCH RELEVANCE

Interferon-γ receptor expression correlated with *MGAT3*/GnT-III expression and poor prognosis in patients with colorectal cancer. Interferon-γ receptor α downregulation was more frequent than programmed death ligand 1 overexpression or *JAK1/2* mutations, and might contribute to refractoriness to checkpoint inhibitors in patients with colorectal cancer. MGAT3 and interferon-γ receptor α expression can be increased in interferon-γ–resistant colorectal cancer cells by pharmacological treatment with all-trans retinoic acid, providing new perspectives to overcome primary immune evasion.

BASIC RESEARCH RELEVANCE

Our results demonstrated the importance of *N*-glycosylation for the interferon-γ response in cancer cells. Defective *N*-glycosylation of interferon-γ receptor α was systematically observed in interferon-γ-resistant colorectal cancer cells, resulting in its proteasome-dependent degradation. The downregulation of MGAT3/GnT-III expression was consistently associated with interferon-γ resistance in colorectal cancer cells, and bisecting glycosylation catalyzed by *MGAT3*/GnT-III was crucial for the stability and function of interferon-γ receptor α.

§ Authors share co-senior authorship.

Current address of Julie Krug: Department of Dermatology, Venereology and Allergology, University Hospital Würzburg, Würzburg, Germany; current address of Gabriele Rodrian: Department of Orthodontics and Orofacial Orthopedics, Universitätsklinikum Erlangen, Friedrich-Alexander-Universität Erlangen-Nürnberg (FAU), Erlangen, Germany; and current address of Philipp Tripal: Optical Imaging Centre Erlangen (OICE), Friedrich-Alexander-Universität Erlangen-Nürnberg (FAU), Erlangen, Germany.

Abbreviations used in this paper: AOM, azoxymethane; ATRA, all-trans retinoic acid; CHO, Chinese hamster ovary; CRC, colorectal carcinoma; DSS, dextran-sulfate sodium; Endo-H, endoglycosidase-H; IFN, interferon; IFNγR, interferon-gamma receptor; ISG, interferon-stimulated gene; JAK, Janus kinase; mRNA, messenger RNA; MSS, microsatellite-stable; PD-1, programmed death 1; PD-L1, programmed death ligand 1; PHA-E, *Phaseolus vulgaris* erythroagglutinin; PHA-L, *Phaseolus vulgaris* phytohemagglutinin-L; PNGase-F, protein-N-glycosidase F; STAT, signal transducer and activator of transcription.

Most current article

0016-5085
https://doi.org/10.1053/j.gastro.2022.11.018

(microsatellite instability–high, MSI).[19,20] On the contrary, microsatellite-stable (MSS) tumors, which represent 85% of sporadic CRCs, show a much lower frequency of JAK1 mutations.[19,21,22] Investigations of an association between CRC prognosis and the absence of expression of either Stat-1 or IFNγRα, at the protein or messenger RNA (mRNA) levels, have yielded contradictory results.[10,23,24] Hence, in the large majority of CRCs, the mechanisms of IFN-γ resistance remain poorly characterized. In the present study, we investigated the mechanisms by which tumor cells inactivate the IFN-γ response, as well as the consequences of such inactivation in terms of tumorigenesis, and whether it is possible to restore IFN-γ sensitivity in CRC tumor cells.

Materials and Methods

Mouse Models of Colon Carcinogenesis

Colitis-associated carcinogenesis was induced in 6- to 8-week-old mice in 2 independent facilities using azoxymethane (AOM) and dextran-sulfate sodium (DSS) with slight protocol variations. Intraperitoneal injection of AOM was performed on day 1 (*Ifngr2*$^{\Delta IEC}$: 10 mg/kg body weight; *Ifngr2*$^{\Delta IEC\text{-}2}$: 12.5 mg/kg body weight) and DSS-containing drinking water (*Ifngr2*$^{\Delta IEC}$: 2%; *Ifngr2*$^{\Delta IEC\text{-}2}$: 2.5% DSS solution) was given for 5 (*Ifngr2*$^{\Delta IEC\text{-}2}$) to 7 (*Ifngr2*$^{\Delta IEC}$) days. DSS supplementation was repeated twice, separated by 14 days of normal drinking water. Animals were killed around day 80. Spontaneous colon carcinogenesis was evaluated in *Ifngr2*$^{\Delta IEC\text{-}2}$*Apc*; *CPC* mice or control mice (*Ifngr2*$^{fl/wt}$*Apc*; *CPC*). Mice were killed at 5 months old. Colon length, tumor number, and diameter were determined macroscopically, and the tumor load was calculated as the cumulative tumor diameter in millimeters per mouse.

Patients

Tissue array. The cohort included patients (n = 416) undergoing surgery at the Universitätsklinikum Erlangen from 1991 to 2001 with follow-up until 2006. Patient and tumor characteristics are given in Supplementary Table 1. Inclusion criteria of the patients were as follows: solitary invasive colon carcinoma (invasion at least of the submucosa) in Union for International Cancer Control stage II–IV, localization >16 cm from the anal verge, no appendix carcinoma, no other previous or synchronous malignant tumor except squamous and basal cell carcinoma of the skin and carcinoma in situ of the cervix uteri, treatment by colon resection with formal regional lymph node dissection, and residual tumor classification R0 (no residual tumor, clinical and histopathological examination). Patients suffering from hereditary CRC or inflammatory bowel disease, patients who died postoperatively, and patients with unknown tumor status (with respect to local and distant recurrence) at the end of the study were excluded.

CRISPR-Cas9 Gene Editing

Single-guide RNAs were designed using Benchling (Biology Software; 2017; retrieved from https://benchling.com). Cloning was performed using the pSpCas9(BB)-2a-Puro (PX459) V2.0 vector (Addgene #62988) and pL-CRISPR.EFS.tRFP vector (Addgene #57819), and confirmed by sequencing. HT-29 cells were transfected with the PX459 plasmid by Lipofectamine 2000 and, 24 hours later, were selected with puromycin for another 72 hours. Afterward, single-cell expansion was performed in a 96-well plate to grow clonal cells. HT-29 cells were then transduced by viral particles generated from the transient transfection of HEK293TN cells with 3 different plasmids encoding VSV-G (pMD2.6, Addgene plasmid 12259), packaging genes (psPAX2, Addgene plasmid 12260) and the pL-CRISPR.EFS.tRFP plasmid. After 72 hours of transduction, the cells were sorted by fluorescence-activated cell sorting for RFP-positivity and single cells were seeded in 96-well plates for further clonal expansion. The clones were screened for knockout of the IFNγRα via Western blotting.

Results

Inhibition of the IFN-γ Response in Intestinal Epithelial Cells Promotes Tumorigenesis

To determine whether the specific loss of sensitivity to IFN-γ by tumor cells influences intestinal tumorigenesis, we generated a mouse model with conditional deletion of the IFN-γ receptor beta chain (IFNγRβ encoded by *Ifngr2*) in intestinal epithelial cells by crossing *Ifngr2*$^{fl/fl}$ mice with *Villin-Cre* mice (Supplementary Figure 1*A*). The resulting *Ifngr2*$^{\Delta IEC}$ mice showed a reduction in *Ifngr2* mRNA expression in colon tissue, and an absence of murine IFNγRβ in colon epithelial cells while the protein was still present in stromal cells (arrows), confirming the specificity of the knockout (Figure 1*A* and *B*). Colon carcinogenesis was induced in *Ifngr2*$^{\Delta IEC}$ and *Ifngr2*$^{fl/fl}$ control mice by treatment with AOM and DSS. *Ifngr2*$^{\Delta IEC}$ mice developed more and larger tumors than *Ifngr2*$^{fl/fl}$ control mice (Figure 1*C*–*F*). This increase in tumorigenesis was not due to an increase in inflammation because *Ifngr2*$^{\Delta IEC}$ mice treated solely with DSS showed less colonic inflammation than control *Ifngr2*$^{fl/fl}$ mice (Supplementary Figure 1*B*–*E*). These results could be replicated independently in another mouse facility using an independent strain (*Ifngr2*$^{\Delta IEC\text{-}2}$, Supplementary Figure 1*F* and *G*). The conditional deletion of *Ifngr2* in a sporadic CRC mouse model (*Apc*;*CPC* mice, which spontaneously develop colon tumors) similarly increased tumor number and load compared with controls (Figure 1*G* and *H*). Hence, genetic mouse models demonstrated that tumor cell intrinsic resistance to IFN-γ increases both colitis-associated and spontaneous colon tumorigenesis.

Loss of IFNγRα Expression Correlates With Decreased Disease-specific Survival in Patients With CRC

The prognostic value of IFN-γ pathway gene expression was assessed in patients with CRC. The mRNA expression of *IFNGR1*, but not *IFNGR2*, *STAT1*, *JAK1,* or *JAK2*, was associated with disease-free survival in The Cancer Genome Atlas cohort (Figure 1*I* and Supplementary Figure 2*A*). These results were confirmed using an independent cohort of patients with CRC, where low *IFNGR1* mRNA expression correlated with a reduced disease-specific survival (Figure 1*J*, Supplementary Table 2). We also observed a modest reduction (less than 2-

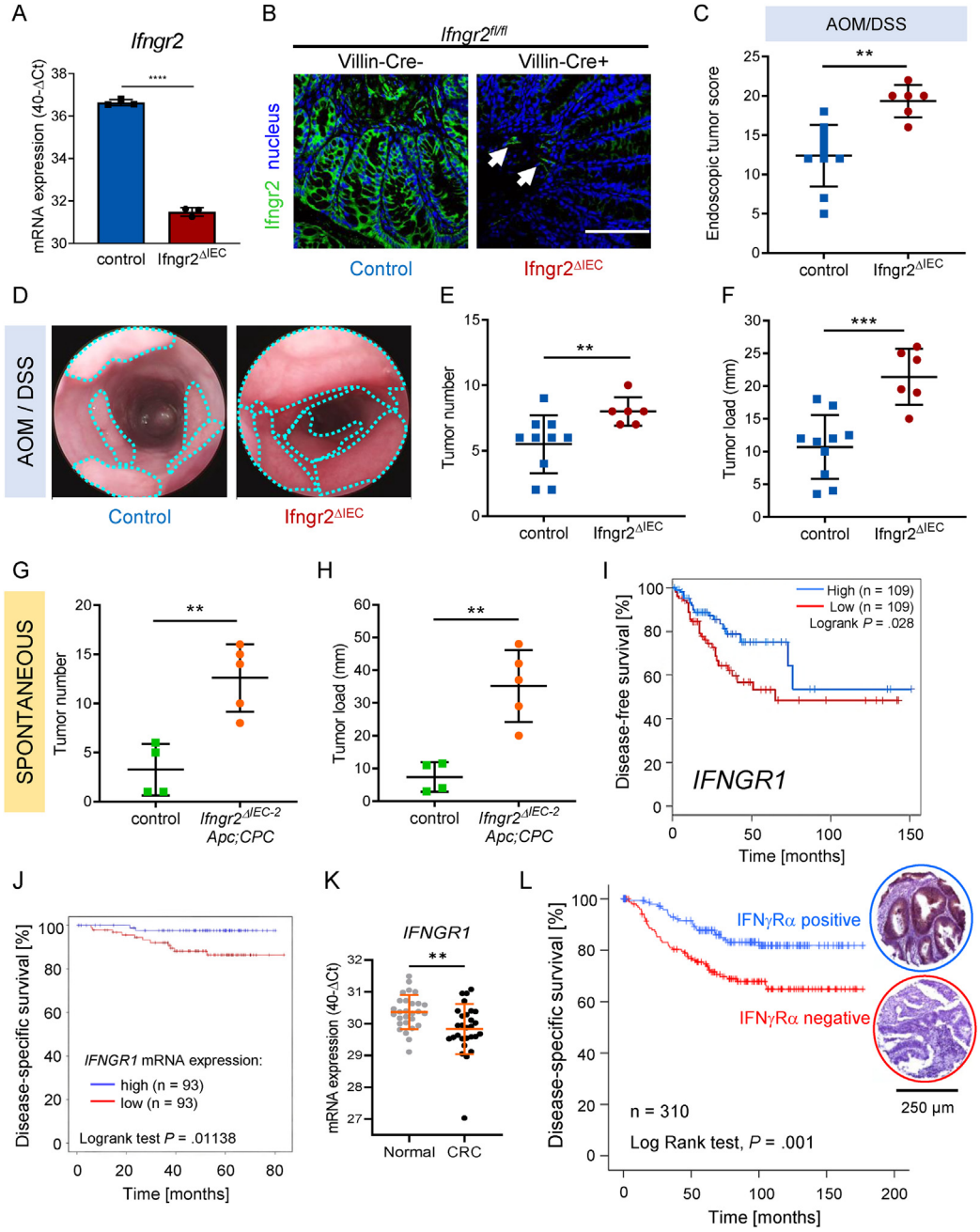

Figure 1. Absence of IFN-γ-receptor expression in colon tumor cells promotes tumorigenesis in mice and correlates with poor prognosis in patients with CRC. (*A*) *Ifngr2* mRNA expression was measured by quantitative reverse transcription polymerase chain reaction (qRT-PCR) in mouse colon tissue in triplicates. Results are given as mean ± SD of 40-ΔCt (Ct_{Ifngr2}-Ct_{Gapdh}) values. Two-tailed unpaired Student *t* test was used for statistical evaluation (*****P* < .0001). (*B*) Representative micrographs of fluorescent immunostaining of IFNγRβ (*green*) in mouse colon tissues. Nuclei were stained with DRAQ5 (*blue*). *Arrows* point at stromal expression of IFNγRβ in otherwise negative colon sections. Scale bar = 100 μm. (*C–F*) Colitis-associated colon carcinogenesis was induced in *Ifngr2*$^{\Delta IEC}$ (n = 6) and control mice (n = 10) by AOM-DSS treatment. Endoscopic scoring (*C*, *D*) and macroscopic evaluation of tumor number (*E*) and tumor load (*F*) are given. Bars represent means ± SD (*C*, *E*, *F*). Two-tailed unpaired Student *t* test (*C*, ***P* = .0014; *F*, ****P* = .0006) or 2-tailed Mann-Whitney test (*E*, ***P* = .0079) were used for statistical evaluation. (*D*) Representative endoscopic pictures showing colonic tumors (*turquoise dotted lines*). (*G* and *H*) Spontaneous colon carcinogenesis was monitored in *Apc;CPC* mice either heterozygous for *Ifngr2* (control, *Ifngr2*$^{+/-}$, n = 4) or devoid of *Ifngr2* in intestinal epithelial cells (*Ifngr2*$^{\Delta IEC\text{-}2}$, n = 5). Two-tailed unpaired Student *t* test was used for statistical evaluation of differences in tumor number (*G*; ***P* = .0029) and tumor load (*H*; ***P* = .0022). (*I*) Kaplan-Meier disease-free survival curve of patients with CRC comparing the 30% highest *IFNGR1* mRNA gene expression samples (*blue*, n = 109) with the 30% lowest (*red*, n = 109; *P* = .028). (*J*) Prognostic value of *IFNGR1* mRNA expression for human patients with CRC (Polyprobe cohort, n = 410). Kaplan-Meier plots of disease-specific survival comparing the 25% highest (*red*, n = 93) and the 25% lowest (*blue*, n = 93) expressing samples (*P* = .01138). (*K*) *IFNGR1* mRNA expression was determined in triplicate by qRT-PCR in corresponding tumor and normal tissues (n = 28). Results are given as 40-ΔCt (Ct_{IFNGR1}-Ct_{RPL37A}) (mean ± SD; Mann-Whitney test, ***P* = .0041). (*L*) Disease-specific survival of patients with colon carcinoma with positive (*blue*, n = 152) and negative (*red*, n = 158) tumor cell IFNγRα protein expression (Kaplan-Meier plot, *P* = .001).

fold) in *IFNGR1* mRNA expression in CRC tissues compared with matching patient normal tissues (Figure 1*K*, Supplementary Table 3). We could confirm that mutations in the IFN-γ response pathway genes are rare in CRC (Supplementary Figure 2*B*) and not related to disease-specific survival (Supplementary Figure 2*C*).

Gene expression analysis in whole tissue mRNA samples is not systematically predictive of protein levels, nor does it allow the specific evaluation of tumor cell–associated expression. Therefore, we analyzed the protein expression of the IFN-γ receptor α chain (IFNγRα, encoded by *IFNGR1*) by immunohistochemistry on a tumor tissue microarray from a cohort of 416 patients with colon cancer (Figure 1*L*, Supplementary Table 1). Overall, the quality criteria for analysis were met in 310 of the 416 tumors. A loss of IFNγRα expression in tumor cells was observed in approximately half of the cases (158 of 310), and was associated with increased tumor size (χ^2 test, $P = .04$), lymph node invasion (χ^2 test, $P < .0001$), extramural venous invasion (χ^2 test, $P < .0001$), distant metastasis (χ^2 test, $P = .019$), and Union for International Cancer Control stage (χ^2 test, $P < .0001$). Furthermore, the absence of IFNγRα expression in tumor cells (n = 158, 50.9%) correlated with a shorter disease-specific survival (Figure 1*L*).

IFNγRα Expression Level and Pattern Correlate With IFN-γ Resistance in CRC Cells

To investigate whether IFNγRα loss correlates with IFN-γ resistance in CRC tumor cells, we examined the induction of ISG expression and cell death by IFN-γ in human CRC cell lines together with IFNγRα expression. Among the 11 cell lines tested, 6 were resistant to IFN-γ–induced cell death, Stat1 phosphorylation and ISG expression (*GBP1*, *IDO1*, *CASP1*) (Figure 2*A* and *B*, and Supplementary Figure 3*A* and 4*B*; resistant cell lines highlighted in red). In the other 5 cell lines (in blue), the induction of cell death by IFN-γ correlated with Stat-1 phosphorylation and ISG expression at the protein and mRNA levels (Figure 2*A* and *B*, and Supplementary Figures 3*A* and 4*B*).

Four of 6 IFN-γ–resistant cell lines (RKO, HCT116, SW480, SW620) displayed a strong reduction in IFNγRα mRNA and protein expression compared with the IFN-γ–sensitive cell lines as shown by Western blotting, intracellular and surface immunofluorescence staining, or flow cytometry (Figure 2*C*–*G*, Supplementary Figures 3*C*, 4*A* and *B*, and 5*C*). The 2 remaining resistant lines (DLD-1 and Caco2) expressed IFNγRα, but the protein was detected with a reduced apparent molecular weight (Figure 2*C* and Supplementary Figure 3*C*). In these cells, intracellular staining revealed a perinuclear accumulation of IFNγRα (Figure 2*D*, arrows), associated with the Golgi apparatus (GM130) but not with the endoplasmic reticulum (calnexin) (Supplementary Figure 5*D* and *E*). The quantification of Golgi-associated IFNγRα localization showed an increase in DLD-1 ($P < .0001$) and Caco2 ($P = .1124$) cells compared with HT-29 cells (Figure 2*E*). Although this finding was indicative of some intracellular retention, the cell surface expression of IFNγRα in both cell lines was similar to that in IFN-γ–sensitive cells (Figure 2*F* and *G*, Supplementary Figure 5*B*). Similar differences in the pattern of IFNγRα expression were observed in CRC tissue extracts (Supplementary Figure 4*C*), including both differences in expression level and apparent molecular size shifts toward lower molecular weight.

In contrast, mRNA and protein expression of the other mediators of the IFN-γ response (*IFNGR2*, *STAT1*, *JAK1,* and *JAK2*) was observed in all cell lines except Caco-2. In the latter, no STAT1 expression was detected at the protein level, and JAK2 mRNA expression was reduced (Supplementary Figures 3*C* and 4*A*). Therefore, Caco-2 cells were excluded from further functional tests with IFNγRα because of the presence of additional defects in the JAK-STAT pathway. According to the data retrieved from the Cancer Cell Line Encyclopedia, few mutations were found for *IFNGR1*, *IFNGR2*, *STAT1*, *JAK1,* and *JAK2* in the 11 cell lines investigated, and they did not correlate with IFN-γ resistance (Supplementary Table 4). Furthermore, independent sequencing of *IFNGR1* mRNA from IFN-γ–resistant cells showed no alteration, indicating that the IFNγRα size shift observed in DLD-1 and Caco-2 cells was not due to a truncating mutation or alternative splicing (Supplementary Table 4). Of note, among the 11 CRC cell lines investigated here, none harbored a frameshift JAK mutation and only 1 resistant line (RKO) exhibited overexpression of programmed death ligand 1 (PD-L1) (Supplementary Figure 3*B*), which was not mutually exclusive with down-regulated IFNγRα expression. Overall, these results suggested that defects in IFNγRα expression or post-translational maturation correlate with IFN-γ resistance in CRC cell lines, whereas other signaling components of the pathway are either not or only marginally involved.

IFNγRα Is Aberrantly Glycosylated in IFN-γ–resistant CRC Cells

To determine whether epigenetic gene silencing may be responsible for the downregulation of *IFNGR1* expression in RKO, HCT116, SW480, and SW620 cells, cells were treated with the DNA methylation inhibitor decitabine. Decitabine treatment led to a modest but statistically significant increase in *IFNGR1* mRNA expression in all 4 cell lines (Figure 3*A*), which was, however, not accompanied by an increase at the protein level (Figure 3*B*).

The expression of IFNγRα was then reconstituted by transfection in RKO, HCT116, SW480, and SW620 cells to explore whether this could restore the IFN-γ response. Although ectopic IFNγRα expression achieved by transfection in RKO, HCT116, SW480, and SW620 cells yielded protein levels comparable to those of the IFN-γ–sensitive control cells (Figure 3*C*), and increased IFNγRα expression at the cell surface (Supplementary Figure 6*A*), it failed to restore the response to IFN-γ (Figure 3*D* and Supplementary Figure 6*B*). In addition, IFNγRα showed a reduced apparent molecular weight (Figure 3*C* and *D* and Supplementary Figure 6*B* and *C*) together with an intracellular accumulation at the Golgi apparatus, similar to what

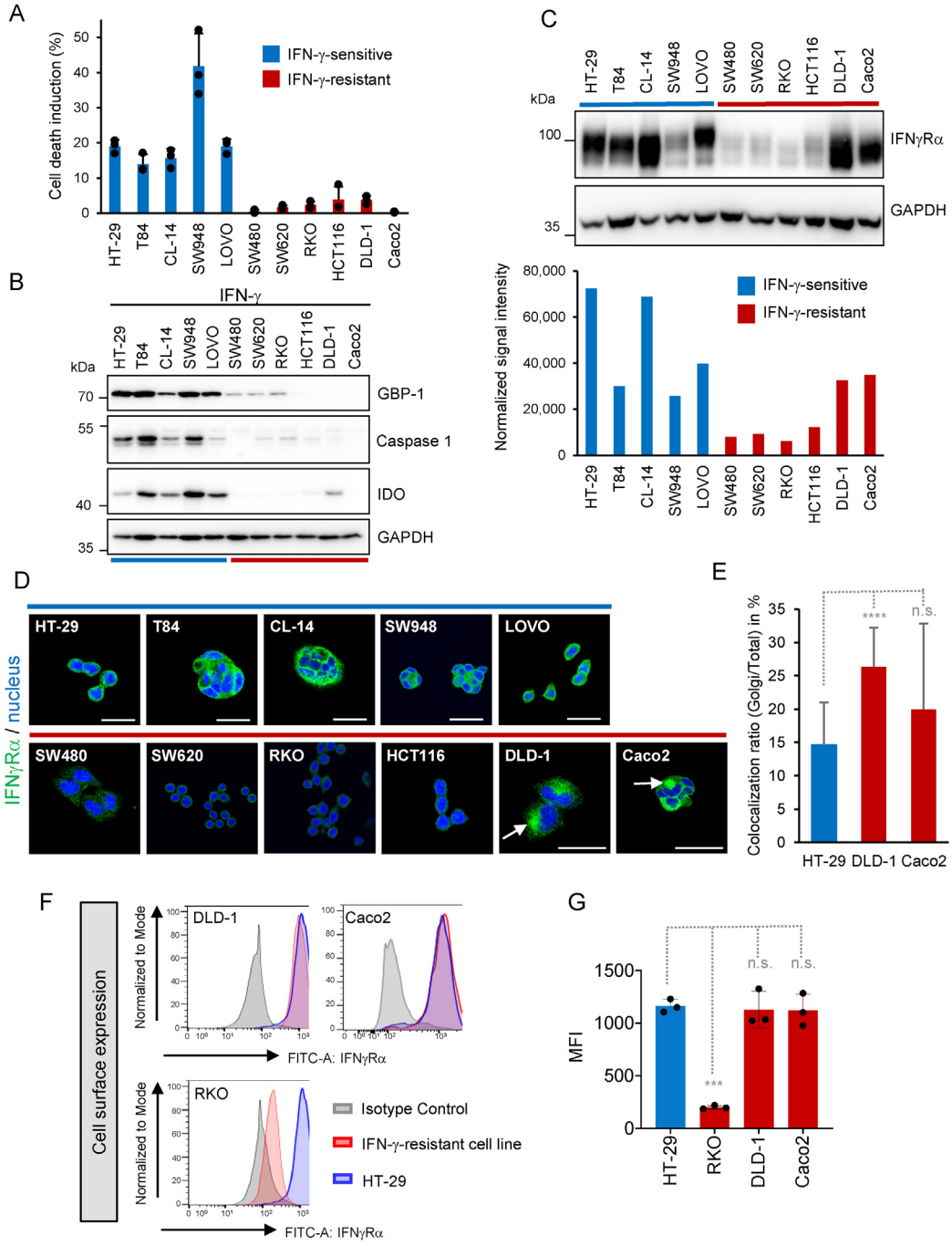

Figure 2. INγRα expression is down-regulated in IFN-γ–resistant cells. IFN-γ–resistant cells are highlighted in *red*, and IFN-γ–sensitive cells in *blue*. GAPDH was used as loading control for Western blots. (*A*) Cell death induction determined 72 hours after IFN-γ treatment (100 U/mL) by flow cytometry. Results are given in percent as the difference between IFN-γ–treated and mock-treated controls (mean ± SD, n = 3 distinct samples). (*B*) ISG expression in CRC cell lines. (*C*) IFNγRα expression in CRC cell lines. (*D*) Intracellular staining of IFNγRα in CRC cells. Nuclei were counterstained with DRAQ5 (*blue*). Scale bars = 25 μm; *arrows* show perinuclear accumulation of IFNγRα. (*E*) Quantification of IFNγRα Golgi localization in HT-29 (n = 14), DLD-1 (n = 19), and Caco-2 (n = 19) cells. (*F*) Cell surface expression of IFNγRα analyzed by flow cytometry in CRC cell lines. IFN-γ–resistant cells (*red*), isotype staining (negative control, *gray*) and HT-29 (positive control, *blue*). (*G*) Mean fluorescence intensity of IFNγRα (MFI) ± SD (n = 3 distinct samples) measured by fluorescence-activated cell sorting in CRC cell lines. Two-tailed unpaired Student *t* test: $^{***}P_{RKO} = .0009$; n.s. = not significant.

was observed in DLD-1 and Caco2 cells (Figure 3*E*, arrows, and Supplementary Figure 6*D* and *E*). The altered migratory pattern and Golgi retention of IFNγRα observed in all IFN-γ–resistant lines, either endogenously or after ectopic expression, suggested differences in *N*-glycosylation.[25] This was supported by the observation of a similar apparent

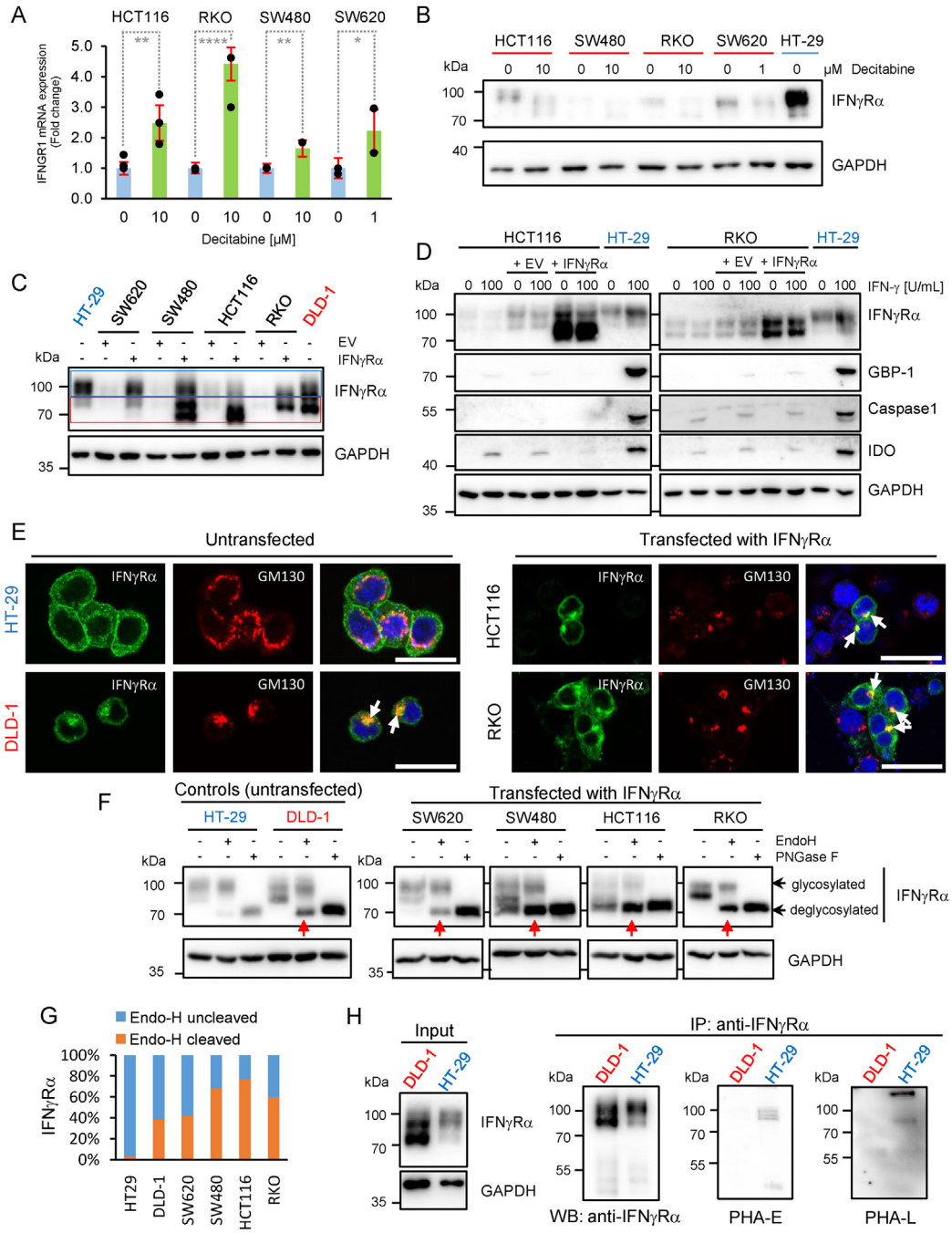

Figure 3. IFNγRα is aberrantly glycosylated in IFN-γ-resistant CRC cell lines. GAPDH was used as loading control for Western blots. (*A*) *IFNGR1* mRNA expression measured in triplicate by quantitative reverse transcription polymerase chain reaction (qRT-PCR) in IFN-γ–resistant cell lines treated with decitabine (1–10 μM) or dimethyl sulfoxide (DMSO) as control for 96 hours. Results are given as fold-change ± SD compared to DMSO-treated control; Student *t* test was performed using ΔCt (Ct_{IFNGR1}-Ct_{RPL37A}) values with $^{**}P_{HCT116} = .0059$, $^{****}P_{RKO} < .0001$, $^{**}P_{SW480} = .0046$, and $^{*}P_{SW620} = .0346$. (*B*) IFNγRα protein expression in CRC cell lines treated with decitabine (1–10 μM) or DMSO as control for 96 hours. (*C* and *D*) IFNγRα and ISG protein expression in SW620, SW480, HCT116, and RKO after transfection with empty vector or IFNγRα-expressing construct. HT29 and DLD-1 cells were used as expression controls. *Rectangles* highlight high (*blue*) and low (*red*) migrating bands. (*E*) Staining of IFNγRα (*green*) and GM130 (*red*) in CRC cells after reconstitution of IFNγRα expression. Nuclei were counterstained with DRAQ5 (*blue*). Scale bar = 25 μm; *arrows* indicate colocalization of IFNγRα and GM130. (*F*) IFNγRα expression in protein lysates from transfected IFN-γ–resistant CRC cells digested with either Endo-H or PNGase-F (each at 1 U/μg protein), lysates processed in absence of enzyme being used as controls. EV, empty vector; IFNγRα, IFNγRα expression plasmid. *Red arrows* indicate digestion of IFNγRα by Endo-H. (*G*) Signal intensity ratio of cleaved and uncleaved IFNγRα in percent of total. (*H*) IFNγRα expression and lectin binding (PHA-E and PHA-L) in immunoprecipitated protein lysates from HT-29 and DLD-1 cells. Input samples (10 μg) were analyzed for IFNγRα expression. WB, Western blot.

molecular weight shift after ectopic expression of the endothelial surface protein Endoglin in IFN-γ–resistant, but not in IFN-γ–sensitive CRC cells (Supplementary Figure 6*F*).

To assess whether IFNγRα was differently glycosylated in IFN-γ–sensitive and –resistant cell lines, we used 2 endoglycosidases with different specificity, protein-*N*-glycosidase F (PNGase-F) and endoglycosidase-H (Endo-H). PNGase-F cleaves all *N*-glycans, whereas Endo-H specifically removes high-mannose *N*-glycan chains (but not mature complex *N*-glycans). PNGase-F treatment resulted in a shift of IFNγRα band size to approximately 70 kDa in all cell lines tested, indicating that the receptor undergoes *N*-glycosylation to some extent in both IFN-γ–sensitive and IFN-γ–resistant cell lines (Figure 3*F*). In IFN-γ–sensitive cells (HT-29), IFNγRα was resistant to Endo-H digestion, indicating a mature complex *N*-glycosylation (Figure 3*F* and *G*). In all IFN-γ–resistant CRC cell lines, IFNγRα was highly sensitive to Endo-H digestion, regardless of whether ectopically (RKO, HCT116, SW480, SW620) or endogenously (DLD-1) expressed, indicating the presence of high-mannose *N*-glycans characteristic of an immature, low-complexity glycosylation.

Endogenously expressed IFNγRα was then immunoprecipitated from HT-29 (IFN-γ–sensitive) and DLD-1 (IFN-γ–resistant) cells, and its modification with complex *N*-glycans was detected by Western blotting using the specific lectins *Phaseolus vulgaris* erythroagglutinin (PHA-E) and *Phaseolus vulgaris* phytohemagglutinin-L (PHA-L). Binding of both PHA-E and PHA-L to IFNγRα was reduced in DLD-1 cells compared with HT-29 cells, indicating a decreased complexity of IFNγRα *N*-glycosylation in IFN-γ–resistant cells (Figure 3*H*).

IFNγRα Stability and Signaling Are Regulated by N-glycosylation

In the next step, we investigated whether changes in *N*-glycosylation were indeed able to affect IFNγRα function. Treatment of IFN-γ–sensitive HT-29 cells with the *N*-glycosylation inhibitors tunicamycin and 2-deoxyglucose induced a shift in the IFNγRα apparent molecular weight and inhibited IFN-γ signaling (Figure 4*A*, Supplementary Figure 7*A*–*C*). We then investigated whether a non-glycosylated form of IFNγRα obtained by mutation of its 5 putative glycosylation sites[25,26] (ΔG-IFNγRα) could signal in response to IFN-γ (Figure 4*B*). As recipient cells, we chose *N*-glycosylation-competent HT-29 cells with a CRISPR-Cas9–mediated knockout of *IFNGR1* (*IFNGR1*-KO HT-29, clone sg 2.21) that exhibited a complete inhibition of IFNγRα protein expression, IFN-γ signaling, and ISG expression compared with controls (NTC) (Figure 4*C* and Supplementary Figure 8*A*–*C*). Ectopic expression of wild-type IFNγRα in *IFNGR1*-KO HT-29 cells resulted in electrophoretic migration at the expected molecular weight (∼90 kDa), as well as induction of pStat-1 phosphorylation, ISG expression, membrane localization, and cell death upon treatment with IFN-γ (Figure 4*D* and Supplementary Figure 8*D*–*H*). In contrast, ectopically expressed ΔG-IFNγRα was detected at approximately 70 kDa by Western blot, below the molecular weight of wild-type IFNγRα and similar to the PNGase-F-treated fully deglycosylated receptor (Figure 4*D*). Contrary to wild-type IFNγRα, ΔG-IFNγRα had a strongly reduced IFN-γ response, both in pools of transduced cells and in single clones (Figure 4*D* and Supplementary Figure 8*D*–*G*). Furthermore, a dose-response analysis suggested that ligand binding of ΔG-IFNγRα is impaired compared with that of wild-type IFNγRα (Supplementary Figure 8*F* and *G*).

To determine whether immature *N*-glycosylation of IFNγRα might increase protein degradation, we treated RKO, HCT116, SW480, and SW620 cells with the proteasome inhibitor MG132. MG132 induced a strong dose-dependent increase in IFNγRα protein levels in all 4 IFN-γ–resistant cell lines (Figure 4*E*), which was, in comparison, not observed in HT-29 cells (Supplementary Figure 8*I*). The protein expression level of ΔG-IFNγRα was also enhanced by treatment with MG132 (Figure 4*F*), confirming that *N*-glycosylation defects can trigger proteasome-dependent degradation of IFNγRα.

Reconstitution of MGAT3 Expression Rescues IFNγRα N-glycosylation and Signaling

To determine which enzymes of the *N*-glycan synthesis pathway might be responsible for the downregulation of IFNγRα complex glycosylation in IFN-γ–resistant CRC cells, a quantitative reverse transcription polymerase chain reaction array was performed (Figure 5*A*). Multiple genes displayed differential expression patterns between IFN-γ–sensitive and –resistant cells. *MGAT3* (N-acetylglucosaminyltransferase III, or GnT-III) was the only gene consistently down-regulated in all IFN-γ–resistant cells compared with IFN-γ–sensitive control cells (HT-29 and SW948; Figure 5*A*, arrow). MGAT3/GnT-III catalyzes the addition of β1,4-linked GlcNAc on the central mannose of the trimannosyl core of *N*-linked oligosaccharides, generating so-called "bisected" *N*-glycans. The downregulation of MGAT3 expression in IFN-γ–resistant cell lines was confirmed at the mRNA and protein levels (Figure 5*C* and Supplementary Figure 9*A* and *B*). In addition, the level of bisected *N*-glycans detected by PHA-E lectin binding correlated with *MGAT3* expression, and was reduced in all IFN-γ–resistant cell lines (Figure 5*B*–*D*).

Therefore, we examined whether the modulation of MGAT3 expression influences IFNγRα complex *N*-glycosylation. Chinese hamster ovary (CHO) cells without MGAT3 activity (Pro-5) or with an MGAT3 gain-of-function mutant (Lec10B cells) were used to ectopically express the IFNγRα protein.[27] Western blot analysis revealed an increased apparent molecular weight and expression level of IFNγRα in Lec10B CHO cells compared with control Pro-5 CHO cells (Supplementary Figure 9*C*), suggesting that MGAT3 activity increases IFNγRα bisected glycosylation and protein levels. All-trans retinoic acid (ATRA) has been shown to increase MGAT3 expression levels and to enhance the addition of bisecting *N*-glycans to proteins in vitro.[28] In the IFN-γ–resistant/MGAT3-low RKO cells, ATRA induced a dose-dependent increase in MGAT3 and IFNγRα protein expression (Supplementary Figure 9*D*; quantification of IFNγRα: middle panel, and MGAT3: lower panel), accompanied by a higher IFNγRα molecular weight

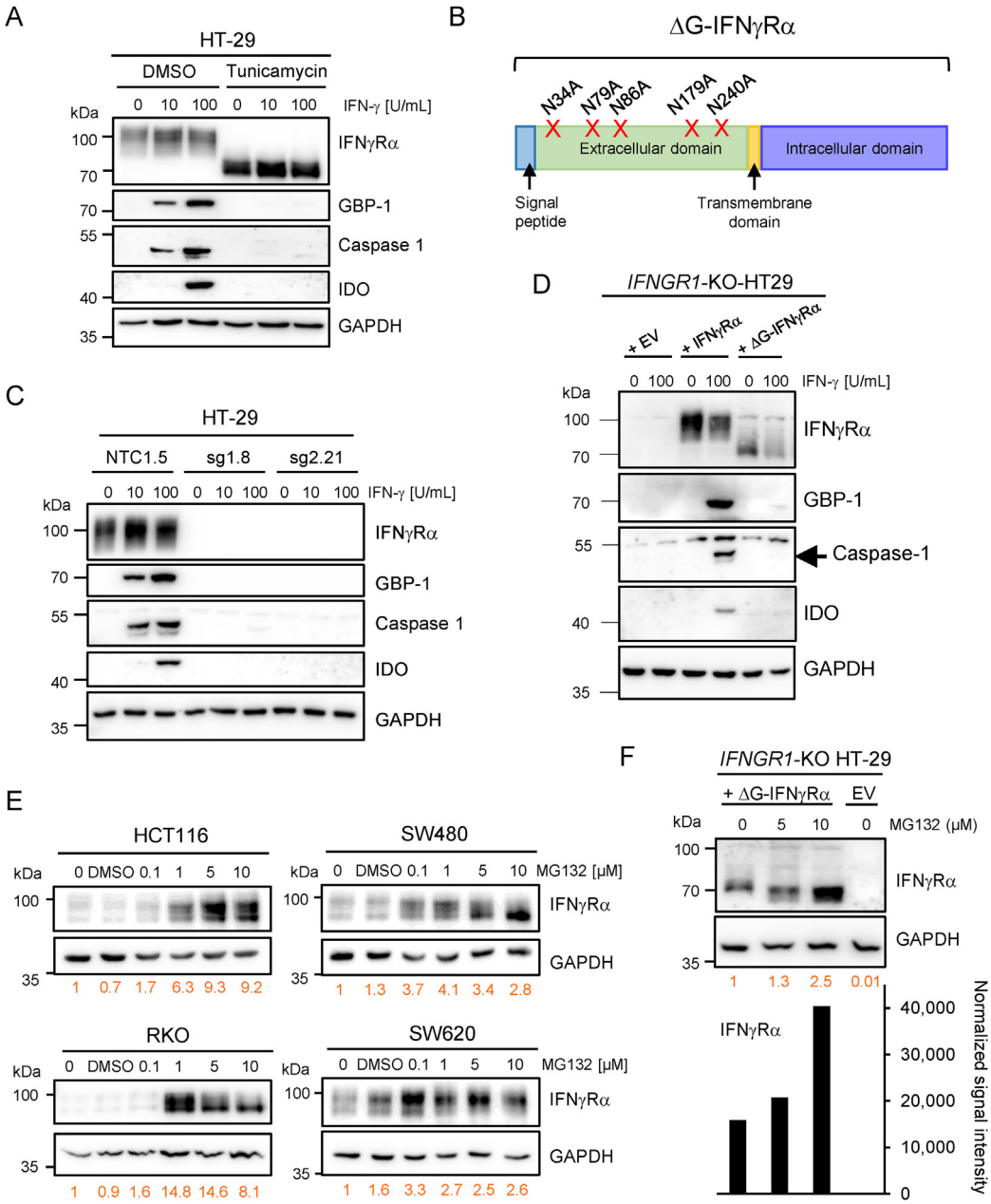

Figure 4. *N*-glycosylation regulates IFNγRα signaling and protein stability in IFN-γ–resistant cells. GAPDH was used as loading control for Western blots. (*A*) IFNγRα and ISG protein expression in HT-29 cells treated with tunicamycin or dimethyl sulfoxide (DMSO) as control for 24 hours before stimulation with IFN-γ. (*B*) Schematic representation of the point mutations inserted in the *IFNGR1* sequence to generate a glycosylation-defective mutant (ΔG-IFNγRα). N, asparagine; A, alanine. (*C*) IFNγRα and ISGs protein expression in *IFNGR1*-KO HT-29 clone sg1.8, sg2.21 and control cells (NTC1.5) after 24 hours of IFN-γ stimulation. (*D*) IFNγRα and ISG expression in *IFNGR1*-KO HT-29 cells transduced with empty virus (EV), wild-type IFNγRα, or the ΔG-IFNγRα. Cells were stimulated for 24 hours with indicated amounts of IFN-γ. (*E*) IFNγRα expression in HCT116, RKO, SW480, and SW620 cell lines treated with increasing concentrations of MG132 (24 hours). The signal intensity for IFNγRα (in *orange*) was normalized to GAPDH intensity and is given relatively to untreated control (set to 1). (*F*) IFNγRα expression in *IFNGR1*-CRISPR KO HT-29 clone sg 2.21 transduced with EV or ΔG-IFNγRα ± increasing concentrations of MG132 (24 hours). IFNγRα signal intensity (*graph*, text in *orange*) was normalized and calculated as in (*E*).

(Supplementary Figure 9*D*; middle panel; green: IFNγRα upper band, gray: IFNγRα lower band), confirming that MGAT3 promotes bisected glycosylation and stabilization of the IFNγRα protein.

The addition of bisecting N-glycans by MGAT3 has been shown to reduce the affinity of cell surface proteins to the galectin lattice, particularly to galectin-3.[29] Consistent with this, the level of bisected *N*-glycans observed on immunoprecipitated endogenous IFNγRα inversely correlated with galectin-3 binding (Figure 3*H* and Supplementary Figure 9*E*), indicating that a reduced MGAT3-dependent addition of bisecting *N*-glycans

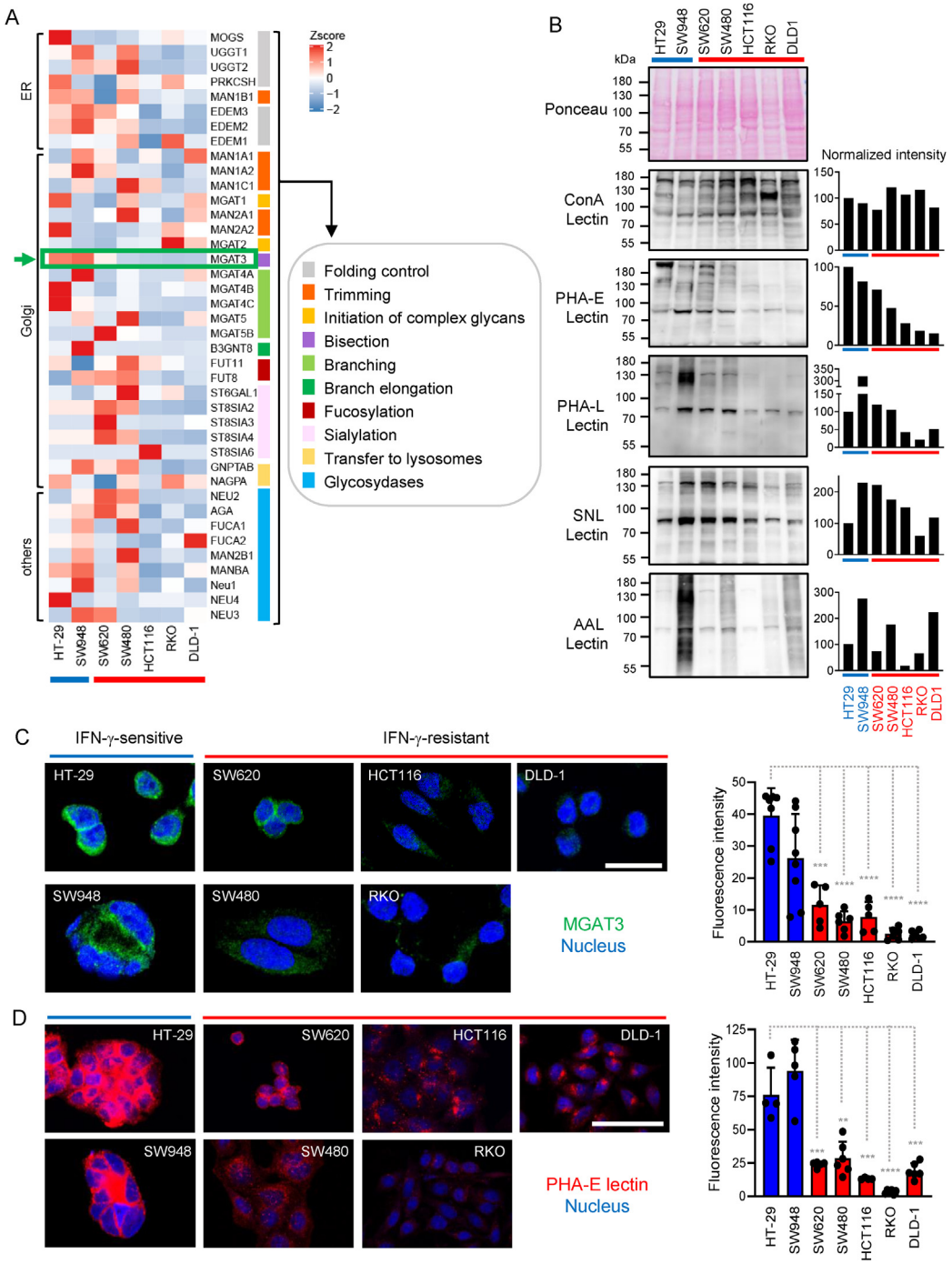

Figure 5. IFN-γ–sensitive and –resistant cells exhibit different *N*-glycosylation profiles. (*A*) Heatmap representation of N-glycosylation gene expression data of IFN-γ–sensitive (*blue*) and IFN-γ–resistant (*red*) CRC cells. Results are depicted as $2^{-}(\Delta Ct_{GOI} - \Delta Ct_{Mean\ GOI})$. (*B*) Lectin blotting analysis of CRC cells (25 μg of protein lysates/lane) was performed using PHA-E, PHA-L, *Sambucus nigra* lectin, and *Aleuria auraentia* lectin lectins. Concanavalin A (ConA) detected the overall level of mannose and glucose residues and was used as control. Ponceau staining was used to verify equal loading. *Bar diagrams* depict intensity values normalized to HT-29 (in percent). (*C*) Staining of MGAT3 (*green*) in CRC cell lines. Nuclei were counterstained with DRAQ5 (*blue*). Scale bar = 25 μm. *Bar diagram* shows mean ± SD of single cell-corrected fluorescence intensity. Two-tailed unpaired Student *t* test was used for comparison between HT-29 (*blue*) and IFN-γ–resistant cell lines (*red*), with $^{***}P_{SW620} = .000105$, $^{****}P_{SW480} < .0001$, $^{****}P_{HCT116} < .0001$, $^{****}P_{RKO} < .0001$, $^{****}P_{DLD\text{-}1} < .0001$. (*D*) CRC cell lines were stained with PHA-E lectin (*red*) and nuclei were counterstained with DRAQ5 (*blue*). Scale bar = 50 μm. *Bar diagram* shows mean ± SD of single cell-corrected fluorescence intensity. Two-tailed unpaired Student *t* test was used for comparison between HT-29 (*blue*) and IFN-γ–resistant cell lines (*red*), with $^{***}P_{SW620} = .0007$, $^{**}P_{SW480} = .0017$, $^{***}P_{HCT116} = .0008$, $^{****}P_{RKO} < .0001$, $^{***}P_{DLD\text{-}1} = .00017$.

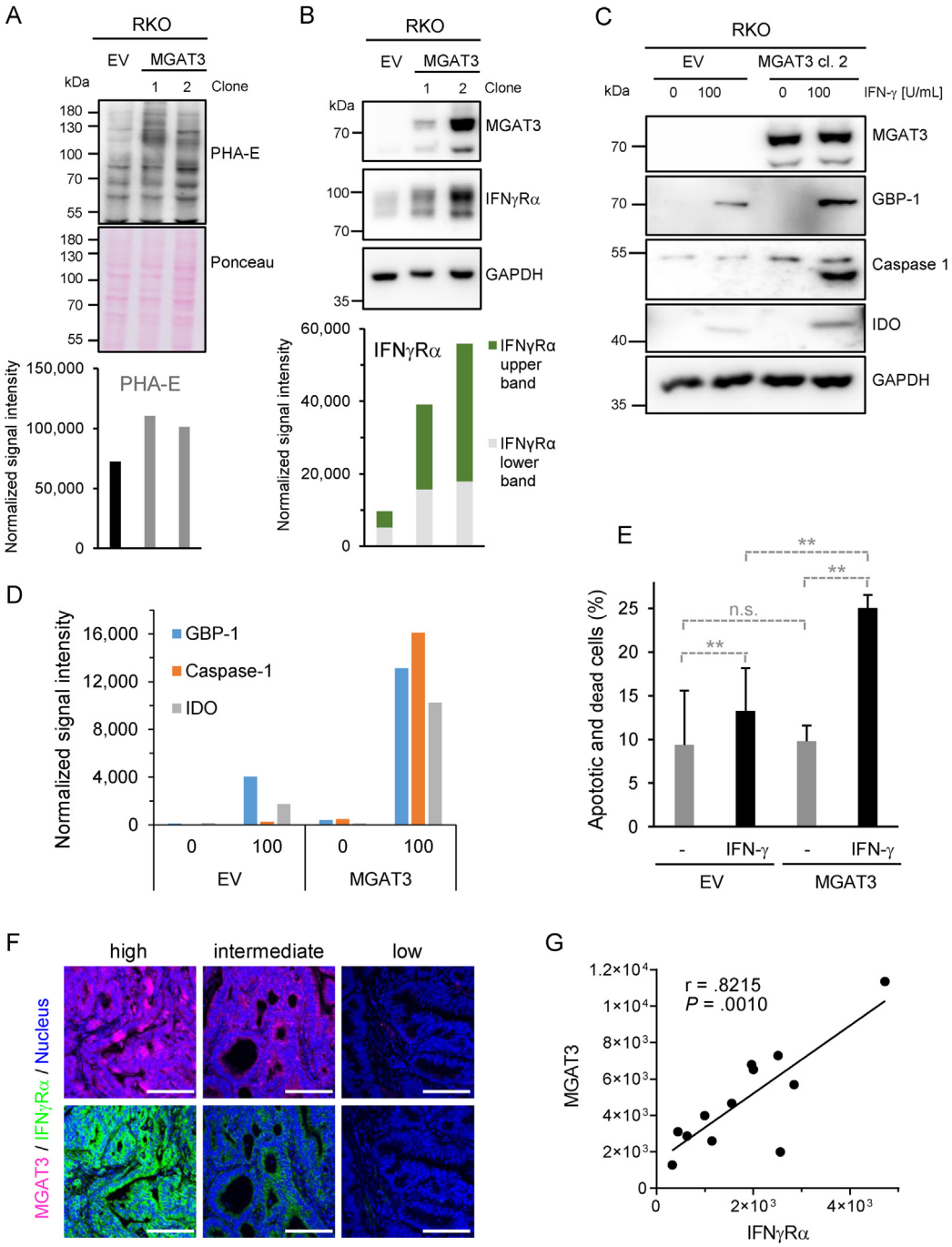

Figure 6. MGAT3 downregulation reduces IFNγRα bisected *N*-glycosylation and signaling. (*A*) PHA-E lectin blotting in RKO cells after stable transfection of *MGAT3* (clone 1 and 2) or empty vector (EV) (25 μg of proteins/lane). Ponceau staining served as loading control and for normalization. (*B*) MGAT3 and IFNγRα protein expression in *MGAT3*-reconstituted RKO clones or RKO-EV. GAPDH was used as loading control and for normalization. Normalized signal intensity IFNγRα is given with upper and lower bands highlighted in *green* and *gray*, respectively. (*C*) MGAT3 and ISG expression in IFN-γ stimulated RKO cells stably transfected with either *MGAT3*-expressing or empty vector (EV). Cells were stimulated with indicated amounts of IFN-γ for 24 h. (*D*) Normalized signal intensity of Western blot in (*C*). (*E*) Cell death induction was determined 72 hours after treatment of RKO-EV/-MGAT3 cells with IFN-γ (0–100 U/ml) by flow cytometry. Results are given in percent of apoptotic and necrotic cells (mean ± SD, n = 3 distinct samples). Student *P* test: n.s., not significant; $^{**}P_{EV+/-IFN-\gamma} = .009$, $^{**}P_{MGAT3+/-IFN-\gamma} = .0031$, $^{**}P_{EV+IFN-\gamma/MAGT3++IFN-\gamma} = .0077$. (*F*) Staining of MGAT3 (*pink*) and IFNγRα (*green*) in consecutive human CRC sections. Scale bars = 100 μm. (*G*) Single tumor-corrected fluorescence intensity of MGAT3 and IFNγRα consecutive staining (n = 12) with Pearson's correlation coefficient *r* and *P* value.

to IFNγRα increases its association with the galectin lattice.

To assess whether the restoration of MGAT3 expression would improve IFNγRα signaling in IFN-γ–resistant cells, we stably expressed MGAT3 in IFN-γ–resistant RKO cells, resulting in a higher level of bisected *N*-glycans (Figure 6*A*, PHA-E). The increase in MGAT3 expression correlated in a dose-dependent manner with an increase in IFNγRα protein levels and a shift toward higher molecular weights as shown in 2 independent clones (cl. 1 and 2) (Figure 6*B*). Most importantly, responsiveness to IFN-γ was restored in the MGAT3-positive cells (cl. 2) compared with the RKO cells transfected with the empty vector (Figure 6*C*–*E*).

To confirm the relevance of our results at the clinical level, we investigated protein expression of MGAT3 and IFNγRα in tumor tissues by immunohistochemistry. A strong positive correlation between MGAT3 and IFNγRα protein levels was observed in human CRC samples (Pearson r = .8215, $P = .001$), which supported our in vitro data (Figure 6*F* and *G* and Supplementary Figure 9*F*).

Finally, we investigated whether the modulation of bisected N-glycosylation might influence colon tumor growth and checkpoint inhibitor therapy. Using a syngeneic colon tumor mouse model, we observed that ATRA treatment reduced tumor growth in 3 of 5 animals (Supplementary Figure 10*A*). The mean tumor diameter was decreased by 28.5% in the ATRA-treated group after 30 days but did not reach statistical significance (Supplementary Figure 10*B* and *C*, $P = .0823$). Anti-PD-1 treatment resulted in complete shrinkage of tumors within 2 weeks, and addition of ATRA reduced the half-life of anti-PD-1 treatment from 3.141 to 1.617 day (Supplementary Figure 10*D*). These results suggested that the addition of ATRA might increase the efficacy of checkpoint inhibitor treatment. Further investigations (eg, using lower anti-PD-1 concentrations) are needed to establish whether ATRA can synergistically improve the efficacy of checkpoint inhibitors.

Discussion

In CRC, the development of an IFN-γ–driven host antitumor immune response positively influences patient survival.[1] However, the clinical benefit of IFN-γ treatment or second-generation immunotherapies, such as immune checkpoint inhibitors, remains limited in CRC, suggesting that primary immune escape is a common event.[16–18,21] Immune evasion driven by frameshift mutations of *JAK1/2* or PDL-1 overexpression, has been described in CRC in association with the microsatellite instability–high subtype, which represents only 15% of sporadic CRCs.[12,13,21] In agreement with our results, both kinds of events remain rare in MSS CRCs, and there is no clinical benefit for anti-PD1 treatment due to the low frequency of PDL-1 overexpression.[19,21,22] In MSS CRCs, up-regulated PDL-1 expression is even associated with high PD-1–negative TIL infiltration, IFN-γ production, and improved survival.[30] Here we described an alternative mechanism of immune evasion mediated by the loss of IFNγRα expression, which occurred more frequently than PD-L1 overexpression or JAK mutations, and correlated with poor survival in patients with CRC. Interestingly, the downregulation of *Ifngr1* in murine colon cancer cells resulted in resistance to checkpoint inhibitor treatment (anti-PD-1) in a syngeneic mouse model,[31] suggesting that the loss of IFNγRα expression also contributes to the intrinsic resistance to checkpoint inhibitor therapy in patients with MSS-CRC.

In our study, all IFN-γ–resistant cells were also *N*-glycosylation deficient. At the cellular level, we found that immature/lack of *N*-glycosylation of IFNγRα increased proteasome-dependent degradation. IFNγRα harbors several ubiquitin acceptor sites and undergoes endogenous ubiquitin-dependent proteasomal degradation.[32] This basal proteasome-dependent protein turnover is not physiologically increased after ligand binding, but is enhanced on Toll-like receptor engagement or in case of viral infection,[32–34] supporting our results and suggesting that IFNγRα expression is down-regulated under pathologic conditions. A similar link between *N*-glycosylation status and proteasomal degradation has been described for several transmembrane proteins including the epidermal growth factor receptor and PDL-1.[35,36] At the molecular level, *N*-glycosylation-deficient IFNγRα could reach the cell surface, but its function was inhibited, in agreement with radioligand binding assays showing that *N*-glycosylation of IFNγRα is necessary for ligand binding, but does not affect membrane transport.[26] Furthermore, we observed that immaturely glycosylated IFNγRα had a much stronger affinity for galectin-3 than the functional receptor, indicative of an association with the galectin lattice that could impair ligand accessibility.[37,38]

In CRC cell lines, downregulation of MGAT3 expression was systematically associated with IFN-γ resistance. In addition, MGAT3 expression correlated with IFNγRα expression in human CRC. The downregulation of MGAT3 expression along with the reduction of bisected *N*-glycans are indeed commonly observed in CRC.[39,40] The reconstitution of MGAT3 expression after either transfection or by treatment with ATRA was sufficient to increase both the bisected *N*-glycan modification and the protein stability of IFNγRα in IFN-γ–resistant cells, restoring its signaling ability. These results are supported by the fact that manipulation of bisected *N*-glycan levels was previously shown to regulate protein turnover, function, and membrane subdomain localization of a number of transmembrane proteins, including the epidermal growth factor receptor, IFNγRβ, and E-cadherin.[38,41,42] In the MC38 xenograft syngeneic tumor model, the downregulation of *Ifngr1* in CRC cells induced resistance to anti-PD-1 treatment,[31] whereas treatment with ATRA resulted in a modest inhibition of tumor growth when applied alone, and reduced the half-life of the anti-PD-1 response by half. Although the use of the MC38 xenograft tumor model to assess a synergistic effect was limited by the very strong and rapid effect of the anti-PD-1 treatment, our data suggested that ATRA might improve the efficacy of checkpoint inhibitor treatment in CRC. This is supported by reports showing that ATRA

cooperates synergistically with IFN-γ to induce apoptosis in tumor cells,[43] and enhances the effects of immunotherapy in metastatic renal cell carcinoma and melanoma models.[44,45] Further studies are warranted to assess the positive impact of ATRA on the response to checkpoint inhibitor therapy in CRC, notably in conditions of immune resistance.

Taken together, our study provides evidence for a new pathway of immune escape in CRC involving decreased bisecting *N*-glycosylation and degradation of IFNγRα. This mechanism, more frequent than PD-L1 overexpression or *JAK1/2* mutations, might explain, at least partially, the low response to IFN-γ treatment or checkpoint inhibitors in patients with CRC.[16–18,21] The modulation of MGAT3 activity represented a 1-step approach to restore sensitivity to IFN-γ, suggesting a new strategy to overcome primary immune evasion and allow a broader use of immunotherapy in CRC, for example through application of ATRA, a molecule already included in the treatment of various solid cancers.[46]

Supplementary Material

Note: To access the supplementary material accompanying this article, visit the online version of *Gastroenterology* at www.gastrojournal.org, and at https://doi.org/10.1053/j.gastro.2022.11.018.

References

1. Galon J, Costes A, Sanchez-Cabo F, et al. Type, density, and location of immune cells within human colorectal tumors predict clinical outcome. Science 2006; 313:1960–1964.
2. Fridman WH, Pages F, Sautes-Fridman C, et al. The immune contexture in human tumours: impact on clinical outcome. Nat Rev Cancer 2012;12:298–306.
3. Schreiber RD, Old LJ, Smyth MJ. Cancer immunoediting: integrating immunity's roles in cancer suppression and promotion. Science 2011;331:1565–1570.
4. **Hoekstra ME, Bornes L**, Dijkgraaf FE, et al. Long-distance modulation of bystander tumor cells by CD8+ T-cell-secreted IFN-γ. Nat Cancer 2020; 1:291–301.
5. Thibaut R, Bost P, Milo I, et al. Bystander IFN-γ activity promotes widespread and sustained cytokine signaling altering the tumor microenvironment. Nat Cancer 2020; 1:302–314.
6. Dunn GP, Koebel CM, Schreiber RD. Interferons, immunity and cancer immunoediting. Nat Rev Immunol 2006;6:836–848.
7. Barrat FJ, Crow MK, Ivashkiv LB. Interferon target-gene expression and epigenomic signatures in health and disease. Nat Immunol 2019;20:1574–1583.
8. **Naschberger E, Croner RS**, Merkel S, et al. Angiostatic immune reaction in colorectal carcinoma: Impact on survival and perspectives for antiangiogenic therapy. Int J Cancer 2008;123:2120–2129.
9. The Cancer Genome Atlas Network. Comprehensive molecular characterization of human colon and rectal cancer. Nature 2012;487:330–337.
10. Simpson JA, Al-Attar A, Watson NF, et al. Intratumoral T cell infiltration, MHC class I and STAT1 as biomarkers of good prognosis in colorectal cancer. Gut 2010;59:926–933.
11. **Mlecnik B, Bindea G, Kirilovsky A**, et al. The tumor microenvironment and Immunoscore are critical determinants of dissemination to distant metastasis. Sci Transl Med 2016;8:327ra326.
12. Le DT, Uram JN, Wang H, et al. PD-1 blockade in tumors with mismatch-repair deficiency. N Engl J Med 2015; 372:2509–2520.
13. **Mandal R, Samstein RM, Lee KW**, et al. Genetic diversity of tumors with mismatch repair deficiency influences anti-PD-1 immunotherapy response. Science 2019;364:485–491.
14. Britzen-Laurent N, Lipnik K, Ocker M, et al. GBP-1 acts as a tumor suppressor in colorectal cancer cells. Carcinogenesis 2013;34:153–162.
15. Pfizenmaier K, Bartsch H, Scheurich P, et al. Differential gamma-interferon response of human colon carcinoma cells: inhibition of proliferation and modulation of immunogenicity as independent effects of gamma-interferon on tumor cell growth. Cancer Res 1985;45:3503–3509.
16. Pavlidis N, Nicolaides C, Athanassiadis A, et al. Phase II study of 5-fluorouracil and interferon-gamma in patients with metastatic colorectal cancer. A Hellenic Cooperative Oncology Group Study. Oncology 1996;53:159–162.
17. Turner PK, Houghton JA, Petak I, et al. Interferon-gamma pharmacokinetics and pharmacodynamics in patients with colorectal cancer. Cancer Chemother Pharmacol 2004;53:253–260.
18. Zeller W, Garbrecht M, Dierlamm J, et al. Phase I-II study of interferon-gamma and eflornithine (DFMO) in patients with advanced renal cell carcinoma, malignant melanoma and colorectal carcinoma. Oncol Rep 1996;3:447–451.
19. Albacker LA, Wu J, Smith P, et al. Loss of function JAK1 mutations occur at high frequency in cancers with microsatellite instability and are suggestive of immune evasion. PLoS One 2017;12:e0176181.
20. **Berg KCG, Eide PW**, Eilertsen IA, et al. Multi-omics of 34 colorectal cancer cell lines—a resource for biomedical studies. Mol Cancer 2017;16:116.
21. Shin DS, Zaretsky JM, Escuin-Ordinas H, et al. Primary resistance to PD-1 blockade mediated by JAK1/2 mutations. Cancer Discov 2017;7:188–201.
22. **Sveen A, Johannessen B, Tengs T**, et al. Multilevel genomics of colorectal cancers with microsatellite instability-clinical impact of JAK1 mutations and consensus molecular subtype 1. Genome Med 2017;9:46.
23. Zhang C, Hou D, Wei H, et al. Lack of interferon-γ receptor results in a microenvironment favorable for intestinal tumorigenesis. Oncotarget 2016;7:42099–42109.
24. **Du W, Hua F**, Li X, et al. Loss of optineurin drives cancer immune evasion via palmitoylation-dependent IFNGR1 lysosomal sorting and degradation. Cancer Discov 2021; 11:1826–1843.
25. Hershey GK, Schreiber RD. Biosynthetic analysis of the human interferon-gamma receptor. Identification of N-linked glycosylation intermediates. J Biol Chem 1989; 264:11981–11988.

26. Fischer T, Thoma B, Scheurich P, et al. Glycosylation of the human interferon-gamma receptor. N-linked carbohydrates contribute to structural heterogeneity and are required for ligand binding. J Biol Chem 1990;265:1710–1717.
27. Stanley P, Sundaram S, Tang J, et al. Molecular analysis of three gain-of-function CHO mutants that add the bisecting GlcNAc to N-glycans. Glycobiology 2005;15:43–53.
28. **Chen C, Diao D**, Guo L, et al. All-trans-retinoic acid modulates ICAM-1 N-glycan composition by influencing GnT-III levels and inhibits cell adhesion and trans-endothelial migration. PLoS One 2012;7:e52975.
29. Miwa HE, Song Y, Alvarez R, et al. The bisecting GlcNAc in cell growth control and tumor progression. Glycoconj J 2012;29:609–618.
30. **Droeser RA, Hirt C**, Viehl CT, et al. Clinical impact of programmed cell death ligand 1 expression in colorectal cancer. Eur J Cancer 2013;49:2233–2242.
31. **Lv C, Yuan D**, Cao Y. Downregulation of interferon-γ receptor expression endows resistance to anti-programmed death protein 1 therapy in colorectal cancer. J Pharmacol Exp Ther 2021;376:21–28.
32. Londino JD, Gulick DL, Lear TB, et al. Post-translational modification of the interferon-gamma receptor alters its stability and signaling. Biochem J 2017;474:3543–3557.
33. Skrenta H, Yang Y, Pestka S, et al. Ligand-independent down-regulation of IFN-γ receptor 1 following TCR engagement. J Immunol 2000;164:3506–3511.
34. Blouin CM, Lamaze C. Interferon gamma receptor: the beginning of the journey. Front Immunol 2013;4:267.
35. Gabius HJ, van de Wouwer M, André S, et al. Down-regulation of the epidermal growth factor receptor by altering N-glycosylation: emerging role of β1,4-galactosyltransferases. Anticancer Res 2012;32:1565–1572.
36. **Li CW, Lim SO**, Xia W, et al. Glycosylation and stabilization of programmed death ligand-1 suppresses T-cell activity. Nat Commun 2016;7:12632.
37. Ferreira IG, Pucci M, Venturi G, et al. Glycosylation as a main regulator of growth and death factor receptors signaling. Int J Mol Sci 2018;19:580.
38. **Blouin CM, Hamon Y, Gonnord P**, et al. Glycosylation-dependent IFN-γR partitioning in lipid and actin nanodomains is critical for JAK activation. Cell 2016;166:920–934.
39. Balog CI, Stavenhagen K, Fung WL, et al. N-glycosylation of colorectal cancer tissues: a liquid chromatography and mass spectrometry-based investigation. Mol Cell Proteomics 2012;11:571–585.
40. **Gebert J, Kloor M**, Lee J, et al. Colonic carcinogenesis along different genetic routes: glycophenotyping of tumor cases separated by microsatellite instability/stability. Histochem Cell Biol 2012;138:339–350.
41. Partridge EA, Le Roy C, Di Guglielmo GM, et al. Regulation of cytokine receptors by Golgi N-glycan processing and endocytosis. Science 2004;306:120–124.
42. **Xu Q, Isaji T**, Lu Y, et al. Roles of N-acetylglucosaminyltransferase III in epithelial-to-mesenchymal transition induced by transforming growth factor beta1 (TGF-beta1) in epithelial cell lines. J Biol Chem 2012;287:16563–16574.
43. Karmakar S, Walle T, Banik N, et al. Treatment with combination of all-trans retinoic acid and interferon-gamma regressed human glioblastoma T98G xenografts in nude mice. Cancer Res 2008;68:4035–4035.
44. **Mirza N, Fishman M**, Fricke I, et al. All-trans-retinoic acid improves differentiation of myeloid cells and immune response in cancer patients. Cancer Res 2006;66:9299–9307.
45. Tobin RP, Jordan KR, Robinson WA, et al. Targeting myeloid-derived suppressor cells using all-trans retinoic acid in melanoma patients treated with Ipilimumab. Int Immunopharmacol 2018;63:282–291.
46. Chen MC, Hsu SL, Lin H, et al. Retinoic acid and cancer treatment. Biomedicine (Taipei) 2014;4:22.

Author names in bold designate shared co-first authorship.

Received March 9, 2022. Accepted November 8, 2022.

Correspondence
Address correspondence to: Nathalie Britzen-Laurent, Department of Surgery, Friedrich-Alexander-Universität Erlangen-Nürnberg, Universitätsklinikum Erlangen, Schwabachanlage 12, 91054 Erlangen, Germany. e-mail: nathalie.britzen-laurent@uk-erlangen.de.

Acknowledgments
The present work was performed in (partial) fulfillment of the requirements for obtaining the degree of Dr. rer. nat. by Julia Krug (née Straube). The authors thank C. Christoph, G. Hoffmann, T. Gass, and C. Flierl for excellent technical assistance and Werner Muller (Division of Infection, Immunity & Respiratory Medicine, University of Manchester, Manchester, United Kingdom) for providing C57BL/6J Ifngr2fl/fl mice. We are also very thankful to Pamela Stanley for generously providing the Pro-5 and LEC10B CHO cells. Special thanks to Regine Schneider-Stock (Institute of Pathology, Friedrich-Alexander University Erlangen-Nuremberg, Erlangen, Germany) and Clemens Neufert (Medical Clinic I, Friedrich-Alexander University Erlangen-Nuremberg, Erlangen, Germany), for providing access to the mini-endoscope (founded by the Rudolf-Bartling Stiftung, Hannover, Germany).

CRediT Authorship Contributions

Julia Krug, PhD (Conceptualization: Equal; Formal analysis: Equal; Investigation: Lead; Methodology: Equal; Visualization: Lead; Writing – original draft: Supporting).
Gabriele Rodrian, BSc (Investigation: Equal; Methodology: Equal).
Katja Petter, MSc (Investigation: Equal; Methodology: Equal).
Hai Yang, MD (Methodology: Equal; Resources: Equal).
Svetlana Khoziainova, PhD (Investigation: Equal; Methodology: Equal).
Wei Guo, PhD (Investigation: Equal; Methodology: Equal).
Alan Bénard, PhD (Methodology: Equal; Resources: Equal).
Susanne Merkel, MD (Data curation: Equal; Formal analysis: Equal).
Susan Gellert, MSc (Investigation: Equal; Methodology: Equal).
Simone Maschauer, PhD (Investigation: Equal; Methodology: Equal).
Monika Spermann, MSc (Investigation: Equal).
Maximilian Waldner, MD (Methodology: Equal; Resources: Equal).
Peter Bailey, PhD (Formal analysis: Equal; Methodology: Equal).
Christian Pilarsky, PhD (Methodology: Equal; Resources: Equal; Writing – review & editing: Equal).
Andrea Liebl, PhD (Methodology: Equal; Resources: Equal).
Philipp Tripal, PhD (Methodology: Equal; Resources: Equal).
Jan Christoph, PhD (Data curation: Equal; Methodology: Equal).
Elisabeth Naschberger, PhD (Formal analysis: Equal; Methodology: Equal; Resources: Equal; Writing – review & editing: Equal).
Roland S. Croner, MD (Resources: Equal).
Vera S. Schellerer, MD (Resources: Equal).
Christoph Becker, PhD (Methodology: Equal; Resources: Equal; Writing – review & editing: Equal).
Arndt Hartmann, MD (Resources: Equal).
Thomas Tüting, PhD (Conceptualization: Equal; Formal analysis: Equal; Methodology: Equal; Resources: Equal).
Olaf Prante, PhD (Conceptualization: Equal; Formal analysis: Equal; Methodology: Equal; Resources: Equal).
Robert Grützmann, MD (Resources: Equal).
Sergei I. Grivennikov, PhD (Conceptualization: Equal; Formal analysis: Equal; Funding acquisition: Equal; Methodology: Equal; Resources: Equal; Supervision: Equal).

Michael Stürzl, PhD (Conceptualization: Lead; Funding acquisition: Lead; Methodology: Equal; Project administration: Lead; Resources: Lead; Supervision: Lead; Writing – review & editing: Lead).

Nathalie Britzen-Laurent, PhD (Conceptualization: Lead; Formal analysis: Equal; Funding acquisition: Lead; Investigation: Lead; Methodology: Equal; Project administration: Lead; Supervision: Lead; Visualization: Lead; Writing – original draft: Lead; Writing – review & editing: Lead).

Conflicts of interest

The authors disclose no conflicts.

Funding

This work was funded by the Deutsche Forschungsgemeinschaft (DFG, German Research Foundation) – Project-ID 292410854 - BR 5196/2-1 to N.B.L., Project-ID 375876048 – TRR 241 subproject A06 to N.B.L. and M.St., Project-ID 429280966 – TRR305 subproject B07 to N.B.L. and B08 to E.N., Project-ID STU 238/10-1 to M.St., Project-ID 190140969 - KFO 257-4 to M.St. and M.W., Project-ID 280163318 - FOR 2438-2 to E.N. and M.St.; by the Interdisciplinary Center for Clinical Research (IZKF) of the Clinical Center Erlangen (ELAN-Fonds project P027 to N.B.L., Project J19 to N.B.L., and D34 to M.St.); by the W. Lutz Stiftung, the Forschungsstiftung Medizin am Universitätsklinikum Erlangen and the Corona-funding initiative of the Bavarian Ministry of Science and Arts (to M.St.); by the National Institutes of Health (NIH) to S.G. (Project ID NIH R01CA227629 and CA218133).

Data Availability

All material and data requests should be submitted to the corresponding author for consideration.

Supplementary Material and Methods

Transgenic Mice

All mice were housed in specific pathogen-free conditions with a 12-hour light cycle and were routinely screened for pathogens according to Federation for Laboratory Animal Science Associations guidelines. Animals had ad libitum access to a standard diet and water.

***Ifngr2*$^{\Delta IEC}$ mice.** C57BL/6J *Ifngr2* floxed mice [*Ifngr2*$^{fl/fl}$ [1,2]] were crossed with *B6.SJL-Tg(Vil-cre)997Gum/J* [*Villin-Cre*].[3] Cre+ male mice were routinely used for breeding. For experiments, sex- and age-matched animals were selected and Ifngr2$^{\Delta IEC}$ were co-housed with Ifngr2$^{fl/fl}$ controls.

***Ifngr2*$^{\Delta IEC\text{-}2}$ mice.** C57BL/6J *Ifngr2* floxed mice *Ifngr2*$^{tm1a(KOMP)Wtsi}$ [4] were crossed with *B6.Cg-Tg(Vil1-cre)1000Gum/J* [*Villin-Cre*].[3] *Ifngr2*$^{tm1a(KOMP)Wtsi}$ mice were generated using C57Bl6 Agouti ES cell line *Ifngr2tm1a(KOMP)Wtsi* generated in KOMP (The Knockout Mouse Project); Stock Number: 057086-UCD;RRID:MMRRC_057086-UCD (https://www.mmrrc.org/catalog/cellLineSDS.php?mmrrc_id=57086; https://www.mousephenotype.org/data/alleles/MGI:107654/tm1a%2528KOMP%2529Wtsi). After the deletion of neo cassette using in vivo β-actin FLP deleter, an IFNgR2 floxed strain was established.

***Ifngr2*$^{\Delta IEC\text{-}2}$*Apc*; *CPC* mice.** *Ifngr2*$^{tm1a(KOMP)Wtsi}$ [4] mice were crossed with CPC;Apc mice (*Apc*$^{loxP/loxP}$ × *CDX2P 9.5-NLS Cre*[5]).

Mouse Model of Acute Colitis

Colitis was induced by a single cycle of DSS treatment (2% in drinking water for 7 days) in *Ifngr2*$^{\Delta IEC}$ mice and respective *Ifngr2*$^{fl/fl}$ controls. Animals were killed after 10 days.

Syngeneic Tumor Mouse Model

MC38 cells (2×10^5) were injected into the right flank of 8-week-old female C57BL/6 mice (Charles River). When tumors reached a diameter of 3 mm, mice were treated with vehicle (dimethyl sulfoxide), ATRA (15 mg/kg, intraperitoneally, thrice weekly) and anti-PD-1 antibody (clone RMP1–14, 250 μg/mouse, intraperitoneally, twice weekly), or both for 3 weeks. Tumor diameter was monitored 3 times a week with a caliper.

Mouse Endoscopy

Endoscopic examination was performed using a high-resolution mini-endoscope (Karl-Storz) under anesthesia (Isoflurane, 2%, 2 L/min, CP-Pharma). Inflammation and tumor scoring (Endoscore) were performed according to Becker et al.[6]

Patients

Polyprobe cohort. Patients (n = 410) with stage Union for International Cancer Control I–IV CRC were recruited prospectively between 2009 and 2012 in the framework of the Polyprobe study. Exclusion criteria included preoperative radiation or chemotherapy, hereditary CRC (familial adenomatous polyposis, hereditary nonpolyposis colorectal cancer), or inflammatory bowel disease (Crohn's disease, ulcerative colitis) and a resection margin R ≥ 1. An overview of the patient cohort is given in Supplementary Table 2; patient data for tumor/normal comparisons are summarized in Supplementary Table 3.

Cells, Plasmids, and Reagents

CRC cell lines. HT-29, T84, SW948, SW480, SW620, RKO, HCT116, DLD-1, and Caco2 were purchased from ATCC, CL-14 and LOVO cells from the DSMZ (Germany). CHO Pro-5 and CHO LEC10B cell lines were a generous gift from P. Stanley (Albert Einstein College of Medicine, New York, NY).[7] HEK293TN cells were a kind gift from C. Pilarsky (Universitätsklinikum Erlangen, Germany). Cells were cultured in the following media (all ThermoFischer Scientific) and in the presence of fetal growth serum (FCS; Merck): HT-29, HCT116 (McCoy's medium+ 10% FCS); LOVO, SW480, and DLD-1 cells (RPMI+10% FCS); T84 and CL-14 (Dulbecco's modified Eagle's medium/F12 + 10% FCS); RKO (minimum essential medium + 10% FCS); Caco2 and HEK293TN (Dulbecco's modified Eagle's medium + 10% FCS); SW620 and SW948 (L-15 + 10% FCS); CHO Pro-5 and CHO LEC10B (Mem-alpha + 10% FCS). Cells were maintained at 37°C with 0%, 5%, or 8.5% CO_2 and 95% humidity and routinely tested for mycoplasma using the MycoAlert Mycoplasma Detection Kit (Lonza). The plasmids pMCV1.4(−) and pMCV2.2-Flag, which contains a gentamycin resistance cassette, were obtained from Mologen. The complementary DNA (cDNA) sequence of IFNGR1 (NM_000416.3) was cloned in-frame into the pMCV1.4(−) using the KpnI and XbaI restriction site. The cDNA sequence of MGAT3 (NM_002409.5) was inserted in-frame into pMCV2.2-Flag using the EcoRV and MfeI restriction site. Reagents used were as follows: IFN-γ (Cat. No. 11040596001, Roche Applied Science), Decitabine (5-Aza-2'-deoxycytidine, A3656, Sigma-Aldrich), MG132 (M7449, Sigma-Aldrich) Tunicamycin (SML1287, Sigma-Aldrich), 2-Deoxy-D-glucose (2-DG, D6134, Sigma-Aldrich), Puromycin (0204.4, Roth), G418 (SLLD5138, Sigma-Aldrich), PNGaseF (P0704S) and Endo-H (P0702S) (both New England Biolabs Inc), AOM (Sigma-Aldrich, A5486), and DSS (MP Biomedicals, 02 16011090).

Immunofluorescent Staining

Murine colon tissues. Immunofluorescent staining was carried out on formalin-fixed paraffin-embedded (FFPE) mouse colon tissues. Antigen retrieval was performed in target retrieval solution pH 9.0 (TRS9, Dako). The following primary antibody was used for 1 hour at room temperature (RT): rabbit polyclonal anti-mouse Ifngr2 (Pineda Antikörper Service; 1:500). AlexaFluor546-conjugated goat anti-rabbit (both 1:500, Thermo Fisher Scientific) was given for 45 minutes at RT.

Intracellular staining of cells. Cells were fixed for 15 minutes in 4% buffered paraformaldehyde and permeabilized in 0.1% Triton X-100 (both purchased at Sigma-Aldrich). Immunocytochemistry was performed as previously described,[8] and the following antibodies were used

for primary staining 5 hours at RT: anti-IFNγRα (sc-700, 1:2000, Santa Cruz Biotechnology), anti-GM130 (Clone 35, 1:1000, BD Biosciences), anti-Calnexin (sc-23954, 1:500, Santa Cruz Biotechnology), anti-GnT-III (A8134, 1:1000, Abclonal). After washing, cells were incubated for 1 hour at RT with the following secondary antibodies (1:500): Alexa Fluor 488-conjugated goat anti-rabbit immunoglobulin (Ig) G and Alexa Fluor 546-conjugated goat anti-mouse IgG (both from Invitrogen).

Surface staining of cells. Cells were seeded 24 hours before start of staining. After initial washing steps and blocking, the primary antibodies (anti-IFNγRα,sc-12755, 1:100) and Concanavalin A (1 μg/mL, Vector Laboratories) were applied for 2 hours at 37 °C. The secondary antibody Alexa Fluor 488-conjugated goat anti-rabbit IgG (1:500) and a streptavidin Alexa Fluor 546-conjugated were applied for 45 minutes at RT.

Lectin staining of cells. Cells were handled similar to the other immunofluorescence stainings; however, instead of a primary antibody, the biotinylated *Phaseolus vulgaris* erythroagglutinin (PHA-E, 0.5 μg/mL, B-1125) was applied for 2 hours at 37°C. After washing of the cells, a streptavidin Alexa Fluor 546-conjugate was applied for 1 hour at RT.

Nuclei were stained with DRAQ5 (1:800, Cell Signaling Technology) and slides were mounted with fluorescence mounting medium (Dako). Pictures were taken with a laser-scanning confocal microscope (TCS SPE, Leica Microsystems, equipped with LAS-LAF software). Single cell-corrected fluorescence intensity was calculated as [integrated intensity – (mean fluorescence of background × area of selected cells)]/cell number in selected area.

Tissue Microarray Staining

Antigen retrieval was performed in target retrieval solution pH 9.0 (TRS9, Dako). Slides were incubated for 1 hour with polyclonal rabbit anti-IFNγRα (1:1500; Santa Cruz; sc-700) at RT. Subsequently, sections were incubated for 30 minutes with a Biotinylated Universal Antibody, followed by 30 minutes of incubation with VECTASTAIN Elite ABC Reagent (both Universal Elite ABC kit, Vector Laboratories). The reaction was developed using the Vector NovaRED Substrate Kit (Vector Laboratories) as peroxidase substrate. Slides were counterstained with Mayer's hemalum (VWR International), mounted in DPX mounting medium (Sigma-Aldrich) and examined by light microscopy (DM6000, Leica Microsystems, equipped with LAS-LAF software).

Transfections

SW620, SW480, HCT116, and RKO cells were transiently transfected with the plasmid pMCV1.4-IFNγRα using Lipofectamine 2000 (Invitrogen) according to the manufacturer's protocol. For the generation of stable RKO cells, this cell line was transfected with the plasmid pMCV2.2-Flag-MGAT3 or the corresponding empty vector and subsequently selected by addition of G418 (3,500 μg/mL). Several independent single-cell clones were expanded per construct. Reconstitution of the respective proteins was confirmed by Western blot.

Stable Transduction

Cells were stably transduced by viral particles generated from transient transfection of HEK293TN cells with 3 different plasmids encoding VSV-g, murine leukemia virus gag-pol genes and the retroviral vector pBABE-Puro encoding human IFNγRα, the glycosylation-defective IFNγRα (ΔG-IFNγRα), or the corresponding empty vector (pBABE), following our previously published protocol.[9]

Western Blot Analysis

Quantification of proteins extracted from cells via RIPA buffer was achieved by a modified Lowry assay (Bio-Rad DC protein assay, Bio-Rad Laboratories GmbH) using bovine serum albumin (B9002S, NEB) as a reference standard. Unless otherwise indicated, 10 μg of total proteins were loaded per lane into a 10% sodium dodecyl sulfate (SDS)-polyacrylamide gel and separated under reducing conditions, before being transferred to a polyvinylidene difluoride membrane (T830.1, 0.45 mm, Roth) and detected as described previously.[8] The following antibodies were used for detection of the different proteins: anti-IFNγRα (sc-700, 1:10,000), anti-Stat1 (sc-345, 1:1000), anti-Caspase-1 (sc-622, 1:200) (all Santa Cruz Biotechnology); anti-GBP-1 (clone 1B1, 1:500); anti-p-Stat1 (Y702, ab29045, Abcam, 1:1000); anti-IDO (D5J4E, 1:200), anti-Jak1 (6G4, 1:1000), β2-microglobulin (D8P1H, 1:1000) (each from Cell Signaling); anti-GnT-III (A8134, Abclonal, 1:1000); anti-IFNγRβ (AF773, R&D Systems, 1:1000); anti-GAPDH (MAB374, Merck, 1:40,000). A donkey anti-rabbit IgG antibody coupled to horseradish peroxidase (HRP), a rabbit anti-rat-HRP antibody (Dako), and a rabbit anti-mouse-HRP antibody (Dako) were used as secondary antibodies at the dilution of 1:5000. Protein detection was performed using the SuperSignal West Pico Plus chemiluminescent substrate detection system (34578, ThermoFischer) and the Amersham Imager600 (GE Healthcare). Ponceau staining or GAPDH detection was used as loading control. Quantification was done using the Fiji software.[10] Signal intensity was determined with the Fiji software and normalized as indicated.

Immunoprecipitation

Cells were seeded into 10-cm culture dishes (Nunc) and harvested by scraping in ice-cold immunoprecipitation lysis buffer (20 mM Tris-HCl, pH 7.5, 150 mM NaCl, 5 mM MgCl2, 1% IGEPAL, supplemented with 1 tablet of Complete Mini EDTA-free protease inhibitor cocktail [Roche] per 10 mL). Protein concentrations were determined using the previously mentioned DC assay (Bio-Rad Laboratories GmbH). One milligram of lysates was pre-cleared via incubation with 25 μL of protein G Plus-protein A agarose suspension (Merck Millipore). For immunoprecipitation, 25 μL of protein G Plus-protein A agarose suspension was preincubated with 2 μg of monoclonal IFNγRα antibody (sc-12755, clone GIR94, Santa Cruz Biotechnology) for 30 minutes at RT and subsequently incubated with pre-cleared lysates overnight on an overhead rotator at 4°C. The next day, beads were washed 5 times for 10 minutes with ice-cold

immunoprecipitation lysis buffer on an overhead rotator. After the final washing step, beads were centrifuged, resuspended in 2 × Laemmli, and boiled for 10 minutes at 95°C. The immunoprecipitated lysates were then subjected to Western blot analysis.

Lectin Blotting

For the detection of different glycan levels on total protein extracts, equal amounts of cellular protein were separated by SDS–polyacrylamide gel electrophoresis and transferred to nitrocellulose membranes (Protran, #1060002, GE Healthcare). Subsequently, a Ponceau staining (P7170, Sigma-Aldrich) was performed 30 minutes at RT to assess equal loading. Depending on the lectin, the membranes were then incubated with 5% milk in 1 × phosphate-buffered saline-0.1% Tween (PBS-T) or 5% bovine serum albumin in 1 × TBS-0.1% Tween (TBS-T) overnight at 4 °C. After 3-times washing with PBS-T or TBS-T, the following biotinylated lectins were applied for 10 minutes at RT: Concanavalin A (ConA, 0.25 μg/mL, B-1005), *Phaseolus vulgaris* erythroagglutinin (PHA-E, 2.5 μg/mL, B-1125), *Phaseolus vulgaris* leucoagglutinin (PHA-L, 2.5 μg/mL, B-1115), *Sambucus nigra* (Bark lectin (SNL, 1 μg/mL, B-1305), and *Aleuria aurantia* lectin (AAL, 1 μg/mL, B-1395) (all purchased from Vector Laboratories). After 3-times washing with PBS-T or TBS-T, membranes were incubated in 1 μg/mL HRP-streptavidin (Vector Laboratories) for 45 minutes at RT. The blots were washed 3 times with PBS-T or TBS-T and subsequently developed using the previously mentioned reagents. Quantification was done using the Image Quant TL software (GE Healthcare).

RNA Isolation

RNA was isolated from eukaryotic cells using the RNeasy Mini Kit (Qiagen) according to the manufacturer's instructions, followed by DNA digestion (DNase, Ambion) and Glycogen precipitation (Thermo Scientific). Concentration of RNA was determined with a Nanodrop 2000c (PeqLab). RNA extraction from FFPE tissue sections was carried out with a fully automated method based on silica-coated iron oxide beads using the VERSANT Tissue Preparation Reagents Kit on Tissue Preparation System (Siemens Healthcare Diagnostics). Total RNA was isolated from 10-μm-thick whole FFPE tissue sections of colon carcinoma samples with a minimum tumor content of 30%.

Quantitative Reverse-Transcription Polymerase Chain Reaction

Quantitative reverse-transcription polymerase chain reaction (qRT-PCR) was performed in triplicate using the SuperScript III Platinum One-Step qRT-PCR kit with ROX (Invitrogen, Life Technologies) according to the manufacturer's instructions with a reverse-transcription time of 30 minutes at 50 °C. PCR reactions were run on a Stratagene/Agilent MX3005P QPCR system (Agilent) using the Versandt kPCR AD software (Siemens). Primers, probes (Eurogentech), and Taqman Assays (Qiagen) used are listed in Supplementary Tables 5 and 6. For RNA isolated from FFPE tissue sections, the housekeeping gene RLP37A was first measured in all extracted RNAs. Subsequently, the RNAs were diluted with nuclease-free water to obtain a cycle threshold (Ct) value of 24 for RPL37a. Diluted RNAs were used for further measurement of IFNGR1. For RNA isolated from cells, 20 ng of total RNA was used.

Glycosylation Array

Reverse transcription of cellular RNA was performed using the RT[2] First Strand kit (Qiagen) according to the manufacturer's protocol. Afterward, the cDNA was analyzed via the RT[2] Profiler Array for Human Glycosylation (PAHS-046Z, Qiagen, optimized for a Stratagene3000xp qRT-PCR machine). The obtained data were run through the Qiagen GeneGlobe Analysis software for normalization with the housekeeping genes GAPDH, HRPT1, and RPLP0. Gene expression was calculated via 2^{-}-(dCT^{GOI}-Mean GOI CT) and heatmaps were generated using the ComplexHeatmap Bioconductor/R package.[11]

Site-directed Mutagenesis

The plasmid pBABE-ΔG-IFNγRα was generated by consecutive site-directed mutagenesis according to the manufacturer's instructions (Quik Change XL Mutagenesis Kit, Stratagene, USA) using the following primers: N38A_5′- TCCTCAGTGCCTACACCAACTGCTGTTACAATTGAATCCTATACC-3′, N79A_5′- TCAGAATGGATTGATGCCTGCATCGCTATTTCTCATCATTATTG-3′, N86A_5′- CAATATTTCTCATCATTATTGTGCTATTTCTGATCATGTTGGTGATCC-3′ , N179A_5′ -CAATGTGTATGTGAGAATGGCCGGAAGTGAGATCCAG-3′, N240A_5′- GTTTGTATTACCATTTTCGCTAGCAGTATAAAAGGTTCTCTTTGG-3′. Mutations in the IFNGR1 gene at the specific sites were confirmed by sequencing.

Omics Data Analysis

Genetic alterations of IFN-γ signaling pathway genes. Four datasets were selected for the analyses of the genetic alterations in IFN-γ signaling pathway genes using cBioPortal (https://www.cbioportal.org/)[12,13]: the DFCI dataset (619 colorectal cancers),[14] the Colorectal Adenocarcinoma TCGA PanCancer dataset (n = 594),[15–21] the MSKCC dataset (1134 metastatic colorectal tumor/normal pairs), and the MSK-IMPACT dataset (339 matched rectal cancer tumor and tumoroid samples).[22] This portal allows for the visualization, analysis, and downloading of large-scale cancer genomic datasets. The genomic alterations included gene mutations and copy number variations (GISTIC). An Oncoprint diagram and disease-specific survival curve were generated according to the online instructions of cBioPortal.

Survival analyses for mRNA expression of IFN-γ signaling pathway genes. The GEPIA (Gene Expression Profiling Interactive Analysis) portal was used to analyze the impact of IFN-γ signaling pathway genes mRNA expression on survival of patients with CRC (http://gepia.cancer-pku.cn/). GEPIA is an interactive web server designed for analyzing the RNA sequencing expression data of 9736 tumors and 8587 normal samples from The Cancer Genome Atlas and the GTEx projects, using a standard

processing pipeline.[23] The relationship between disease-free survival and IFN-γ signaling pathway genes mRNA expression in patients with colorectal cancer (COAD and READ) was depicted by Kaplan-Meier plotting according to the online instructions of GEPIA. Patients with CRC were categorized into 2 groups corresponding to the 30% lowest and the 30% highest expression values of IFN-γ signaling pathway genes. Log-rank test results with $P < .05$ were regarded as statistically significant.

Flow Cytometry

Cells were seeded in the bottom of a 6-well plate (Nunc) and treated with IFN-γ as indicated. Apoptosis was detected 72 hours after treatment using the FITC Annexin V Apoptosis Detection kit I (BD Biosciences) according to the manufacturer's instructions. Flow cytometry was performed using a FACSCalibur cytometer equipped with the CellQuestPro software (BD Biosciences) or a FACSFortessa cytometer equipped with the FACSDiva software (BD Biosciences). Data analysis was done with the FlowJo software (BD Biosciences). Cell death was determined as the percentage of cells positive for FITC Annexin V and/or propidium iodide. Cell death induction was calculated as the difference (in %) between treated and untreated cells.

To determine surface expression of the IFNγRα protein on CRC cell lines, the cells were washed twice with PBS and incubated for 20 minutes at 4°C with primary antibody (anti-IFNγRα, 1:200, sc-12755, mouse IgG2, Santa Cruz Biotechnology) or corresponding isotype control (mouse IgG2, MAB004, R&D Systems). After 2 additional washing steps with PBS, a secondary antibody (Alex Fluor 488-conjugated goat anti-mouse IgG, Invitrogen) was applied for 20 minutes at 4°C in the dark. The staining was terminated with 2 times PBS washing and the cells were analyzed using the FACSCelesta cytometer and the FlowJo software (BD Biosciences).

Statistics

Experimental data. In case of normally distributed data, pairwise comparisons were statistically analyzed using 2-tailed, unpaired or paired Student t test. In case of non-normally distributed data, 2-tailed Mann-Whitney U test was used. Data correlation was assessed using the Pearson's correlation coefficient and test. The GraphPad Prism software version 8.00 (GraphPad Software) was used for all analyses. P values of less than .05 were considered significant and error bars represent ± standard deviation (SD) in all graphs.

Clinical data. The Kaplan-Meier method was used to calculate 5-year rates of disease-specific survival. Log-rank test was used for comparisons of survival. Analyses were performed using SPSS software version 24 (IBM) for the tissue microarray and with the TranSMART platform version 16.2 (24) for the Polyprobe cohort. A P value of less than .05 was considered to be statistically significant. Frequency distributions were compared using the χ^2 test.

Study Approval

Animal experiments performed with *Ifngr2*$^{\Delta IEC}$ mice were in accordance with German law and approved by the Institutional Animal Care and Use Committee of the University of Erlangen and the Animal Experiment Committee of the State Government of Lower Franconia, Würzburg, Germany. *Ifngr2*$^{\Delta IEC\text{-}2}$ and *Ifngr2*$^{\Delta IEC\text{-}2}$*Apc*; *CPC* mice were approved for experiments by the Fox Chase Cancer Center IACUC, Philadelphia, PA. Syngeneic mouse models were approved the Animal Experiment Committee of the State Government of Sachsen-Anhalt, Magdeburg, Germany.

All studies including patients were approved by the ethics committee of the University Hospital of Erlangen. All participants were informed personally and provided written informed consent for this study. Patients' data were pseudonymized and all analyses were carried out in accordance with the Helsinki declaration.

Supplementary References

1. Lee HM, Fleige A, Forman R, et al. IFNgamma signaling endows DCs with the capacity to control type I inflammation during parasitic infection through promoting T-bet+ regulatory T cells. PLoS Pathog 2015;11:e1004635.
2. Villegas-Mendez A, Strangward P, Shaw TN, et al. Gamma interferon mediates experimental cerebral malaria by signaling within both the hematopoietic and nonhematopoietic compartments. Infect Immun 2017;85:e01035–01016.
3. Madison BB, Dunbar L, Qiao XT, et al. Cis elements of the villin gene control expression in restricted domains of the vertical (crypt) and horizontal (duodenum, cecum) axes of the intestine. J Biol Chem 2002;277:33275–33283.
4. Ingram JP, Tursi S, Zhang T, et al. A nonpyroptotic IFN-γ-triggered cell death mechanism in nonphagocytic cells promotes salmonella clearance in vivo. J Immunol 2018;200:3626–3634.
5. Hiroi M, Mori K, Sekine K, et al. Mechanisms of resistance to interferon-gamma-mediated cell growth arrest in human oral squamous carcinoma cells. J Biol Chem 2009;284:24869–24880.
6. Becker C, Fantini MC, Neurath MF. High resolution colonoscopy in live mice. Nat Protoc 2006;1:2900–2904.
7. Stanley P, Sundaram S, Tang J, et al. Molecular analysis of three gain-of-function CHO mutants that add the bisecting GlcNAc to N-glycans. Glycobiology 2005;15:43–53.
8. **Ostler N, Britzen-Laurent N**, Liebl A, et al. Gamma interferon-induced guanylate binding protein 1 is a novel actin cytoskeleton remodeling factor. Mol Cell Biol 2014;34:196–209.
9. Naschberger E, Wenzel J, Kretz CC, et al. Increased expression of guanylate binding protein-1 in lesional skin

of patients with cutaneous lupus erythematosus. Exp Dermatol 2011;20:102–106.
10. Schindelin J, Arganda-Carreras I, Frise E, et al. Fiji: an open-source platform for biological-image analysis. Nat Methods 2012;9:676–682.
11. Gu Z, Eils R, Schlesner M. Complex heatmaps reveal patterns and correlations in multidimensional genomic data. Bioinformatics 2016;32:2847–2849.
12. Cerami E, Gao J, Dogrusoz U, et al. The cBio cancer genomics portal: an open platform for exploring multidimensional cancer genomics data. Cancer Discov 2012;2:401–404.
13. Gao J, Aksoy BA, Dogrusoz U, et al. Integrative analysis of complex cancer genomics and clinical profiles using the cBioPortal. Sci Signal 2013;6:pl1.
14. Giannakis M, Mu XJ, Shukla SA, et al. Genomic correlates of immune-cell infiltrates in colorectal carcinoma. Cell Rep 2016;15:857–865.
15. Ellrott K, Bailey MH, Saksena G, et al. Scalable open science approach for mutation calling of tumor exomes using multiple genomic pipelines. Cell Syst 2018;6:271–281.e277.
16. Bhandari V, Hoey C, Liu LY, et al. Molecular landmarks of tumor hypoxia across cancer types. Nat Genet 2019;51:308–318.
17. Hoadley KA, Yau C, Hinoue T, et al. Cell-of-origin patterns dominate the molecular classification of 10,000 tumors from 33 types of cancer. Cell 2018;173:291–304.e296.
18. Liu J, Lichtenberg T, Hoadley KA, et al. An integrated TCGA pan-cancer clinical data resource to drive high-quality survival outcome analytics. Cell 2018;173:400–416.e411.
19. Sanchez-Vega F, Mina M, Armenia J, et al. Oncogenic signaling pathways in The Cancer Genome Atlas. Cell 2018;173:321–337.e310.
20. Taylor AM, Shih J, Ha G, et al. Genomic and functional approaches to understanding cancer aneuploidy. Cancer Cell 2018;33:676–689.e673.
21. Gao Q, Liang WW, Foltz SM, et al. Driver fusions and their implications in the development and treatment of human cancers. Cell Rep 2018;23:227–238.e223.
22. Vasaikar S, Huang C, Wang X, et al. Proteogenomic analysis of human colon cancer reveals new therapeutic opportunities. Cell 2019;177:1035–1049.e1019.
23. Tang Z, Li C, Kang B, et al. GEPIA: a web server for cancer and normal gene expression profiling and interactive analyses. Nucleic Acids Res 2017;45:W98–W102.
24. Athey BD, Braxenthaler M, Haas M, et al. tranSMART: an open source and community-driven informatics and data sharing platform for clinical and translational research. AMIA Jt Summits Transl Sci Proc 2013;2013:6–8.

Author names in bold designate shared co-first authorship.